Active Deformation Processes in Alaska, Based on 15 Years of GPS Measurements

Jeffrey T. Freymueller,[1] Hilary Woodard,[2] Steven C. Cohen,[3] Ryan Cross,[4] Julie Elliott,[1] Christopher F. Larsen,[1] Sigrún Hreinsdóttir,[5] and Chris Zweck[6]

We present a comprehensive average velocity field for Alaska, based on repeated GPS surveys covering the period 1992–2007, and review the major results of previously published papers that used subsets of this data. The spatially and temporally complex pattern of crustal deformation in Alaska results from the superposition of several processes, including postseismic deformation after the 1964 earthquake, spatial variations in plate coupling/slip deficit, translation and rotation of large crustal blocks or plates, and a large slow-slip event in Cook Inlet. Postseismic deformation from the 1964 earthquake continues today, mainly caused by viscoelastic relaxation, and causes trenchward motion. The behavior of the shallow seismogenic zone along the Alaska–Aleutian megathrust is characterized by dramatic along-strike variability. The width of the inferred seismogenic zone varies over along-strike distances that are short compared to the width. The along-strike distribution of locked and creeping regions along the megathrust is consistent with the persistent asperity hypothesis. A large slow-slip event occurred in upper Cook Inlet in 1998–2001, and a smaller event in the same area in 2005–2006. No sign of slow-slip events has been found in segments that are dominated by creep, which suggests that creep there occurs quasi-statically. The overriding plate in Alaska is subject to considerable internal deformation, and can be described in terms of the independent motions of at least four blocks: the Bering plate, the Southern Alaska block, the Yakutat block, and the Fairweather block.

[1]Geophysical Institute, University of Alaska Fairbanks, Fairbanks, Alaska, USA.

[2]Formerly at Geophysical Institute, University of Alaska Fairbanks, Fairbanks, Alaska, USA.

[3]Formerly at NASA Goddard Space Flight Center, Greenbelt, Maryland, USA.

[4]Now at Tetra Tech Inc., Seattle, Washington, USA.

[5]Department of Geosciences, University of Arizona, Tucson, Arizona, USA.

[6]Department of Hydrology and Water Resources, University of Arizona, Tucson, Arizona, USA.

Active Tectonics and Seismic Potential of Alaska
Geophysical Monograph Series 179

10.1029/179GM02

1. INTRODUCTION

Southern Alaska is a tectonically complex region where abundant seismicity is produced by the interaction of the Pacific and North American plates. Over most of the region (Figure 1), the Pacific plate subducts beneath the North American plate, producing a classic Wadati–Benioff zone of intermediate earthquakes, and giving rise to extremely large megathrust earthquakes. These shallow events include 3 of the 10 largest earthquakes ever recorded, led by the 1964 Great Alaska earthquake (M_w = 9.2). The bathymetric expression of the Aleutian trench ends near the east end of the 1964 earthquake rupture zone, but convergence between the plates continues over an additional 250-km segment to the east, at which point the boundary becomes a transform

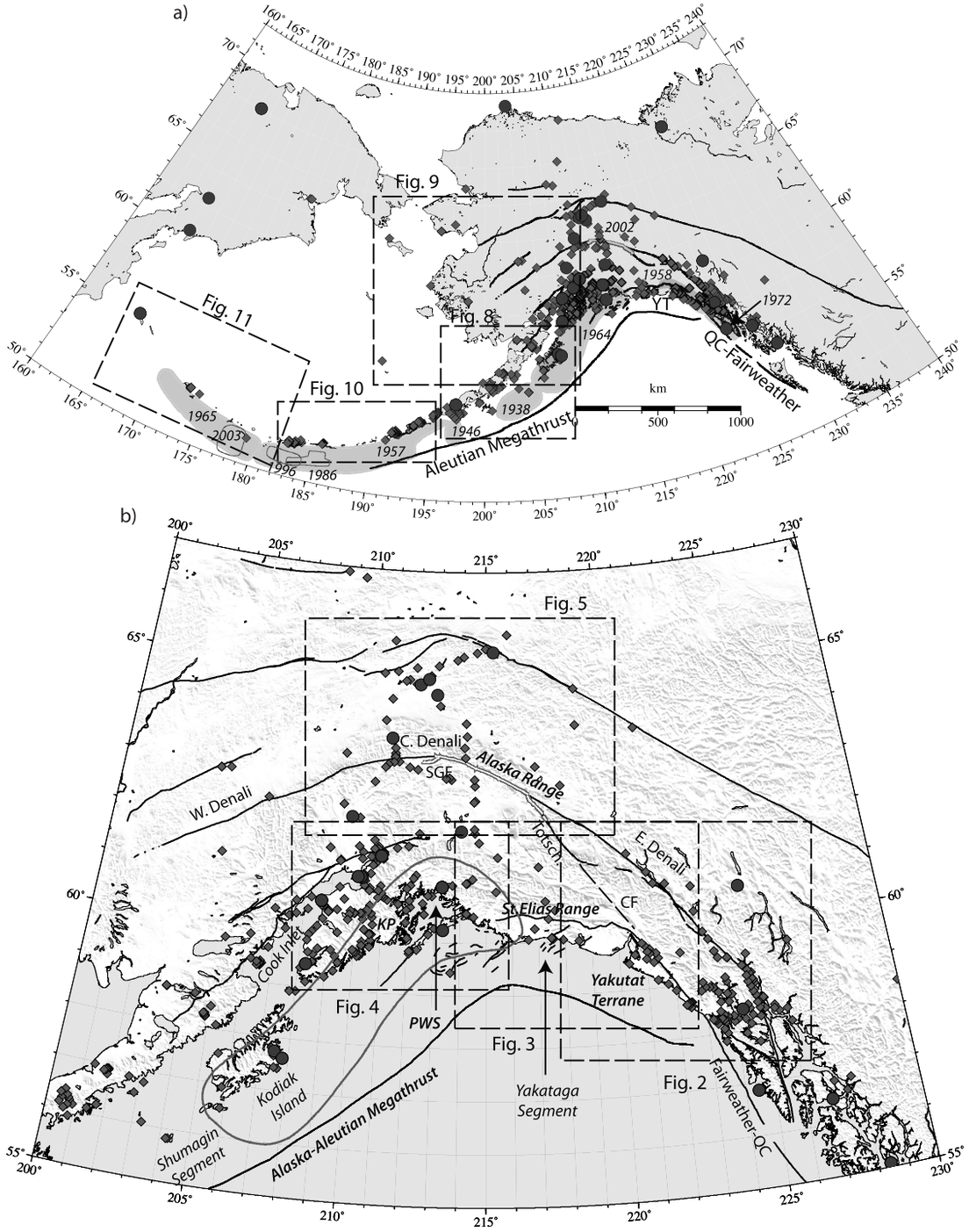

Figure 1. Location map showing major Quaternary active faults [*Plafker et al*., 1994], sites with GPS velocities, and the area of other figures. Faults shown with solid lines, small diamonds are sites with campaign surveys, and larger circles are continuous GPS sites. (a) All of Alaska, with outline area of other figures shown by dashed lines. Shaded regions show the rupture zones of great earthquakes, labeled by their year of occurrence. Outlined areas within the 1957 and 1965 earthquake rupture zones show the rupture areas of the $M \sim 8$ 1986, 1996, and 2003 earthquakes. (b) Blowup view of region of densest data. The rupture areas of the 1964 Alaska earthquake and the 2002 Denali fault earthquake are outlined. YT, Yakutat terrane; PWS, Prince William Sound; KP, Kenai Peninsula; SGF, Susitna Glacier Fault.

boundary that continues down the Pacific coast of Alaska and Canada to Vancouver Island on the Fairweather and Queen Charlotte faults.

The Chugach–St. Elias Range lies along the coast of southern Alaska in the gap between the subduction boundary to the west and the transform boundary to the east. These high and steep mountains lie at the northern boundary of the Yakutat terrane, an exotic terrane in the process of accreting to North America (Figure 1a). The Yakutat terrane moved north with the Pacific plate, and began to collide with North America at ~6 Ma [*Plafker and Berg*, 1994]. The Yakutat terrane consists either of a combination of continental and oceanic crust, or thickened oceanic crust [*Pavlis et al.*, 2004]; in either case, it is buoyant and appears to resist subduction. The Yakutat terrane thrusts under the St. Elias Range (Figure 1b), and to the west it underthrusts Prince William Sound [*Eberhart-Phillips et al.*, 2006; *Plafker and Berg*, 1994]. Subducted Yakutat crust may extend beneath North America as much as 500 km northwest from the trench [*Eberhart-Phillips et al.*, 2006; *Ferris et al.*, 2003]. A more complete description of the Yakutat terrane collision and subduction is given by *Chapman et al*. [this volume].

The southern Alaska margin features a wide zone of deformation inboard of the megathrust. The most intense inboard deformation occurs in a band that extends north and west of the St. Elias Range, where the impact of the Yakutat terrane has had the greatest effect. The right-lateral strike-slip Denali fault curves northwestward, well inboard of the St. Elias, and bounds a block of southern Alaska crust that rotates about a pole near Prince William Sound [*Fletcher*, 2002; *Lahr and Plafker*, 1980; *St. Amand*, 1957; *Stout and Chase*, 1980]. The central part of the Denali fault shows abundant Holocene offset features consistent with a slip rate of several mm/yr or faster over much of its length [*Matmon et al.*, 2006; see also *Haeussler*, this volume]. The Denali fault system also includes a southeastern splay called the Totschunda fault, which may be part of an active connection between the Fairweather fault system in SE Alaska and the central Denali fault [*Kalbas et al*., this volume; *Richter and Matson*, 1971]. The 2002 Denali Fault Earthquake ruptured almost 300 km of the Denali and Totschunda faults, after initiating on the Susitna Glacier thrust [*Crone et al*., 2004; *Eberhart-Phillips et al.*, 2003; *Haeussler et al.*, 2004; *Hreinsdóttir et al.*, 2006].

1.1. Terrestrial Geodetic Measurements

The USGS established several terrestrial geodetic networks in Alaska in the early 1980s. They repeated surveys of triangulation points [*Lisowski et al.*, 1987; *Savage et al.*, 1981], and carried out repeated electronic distance measurement (EDM) line-length surveys of networks crossing the Denali, Totschunda, and Fairweather faults, and networks to study the strain associated with subduction in the Yakataga and Shumagin segments (Figure 1b) [*Lisowski et al.*, 1988; *Savage and Lisowski*, 1986, 1988, 1991].

The results of this work for the strike-slip faults were mixed. The EDM data from the Fairweather fault showed that the slip rate must be very high, although a precise rate could not be determined without independently constraining the locking depth [*Lisowski et al.*, 1987]. A repeat survey of a triangulation network crossing the Totschunda fault also revealed right-lateral strain consistent with a slip rate of 10 ± 5 mm/yr [*Lisowski et al.*, 1987]. Work on the Denali fault was less successful. During the 1980s, it was commonly thought that the Denali fault might have a slip rate almost comparable to the San Andreas fault, 10–20 mm/yr or more [*Plafker et al.*, 1977]. However, two EDM networks across the fault showed nearly negligible shear strain, but significant fault-normal extension [*Savage and Lisowski*, 1991]. Still, given the error bars of the EDM measurements, the low right-lateral shear strain rate is not in conflict with later GPS measurements, because the EDM measurements were made very close to the fault. It is possible that some of the fault-normal extension was due to postseismic deformation after the 1964 earthquake (H. Suito and J. T. Freymueller, A viscoelastic and afterslip postseismic deformation model for the 1964 Alaska earthquake, submitted to *J. Geophys. Res*., 2008, hereinafter referred to as Suito and Freymueller, submitted manuscript, 2008), although geodetic monument instability or systematic errors are also possible explanations.

The network in the Yakataga segment (Figure 1b) showed rapid contractional strain with only small deviations from uniform uniaxial contraction. A simple subduction-type dislocation model could explain the observed deformation reasonably well, as long as the direction of plate convergence was taken to be N36°W instead of the N15°W direction of Pacific–North America relative motion [*Savage and Lisowski*, 1988]. Although this was not recognized at the time, later GPS measurements showed that the motion of the Yakutat terrane relative to North America was oriented very close to N36°W, and the strain in this region probably reflects Yakutat–North America motion [*Fletcher and Freymueller*, 1999, 2003].

The EDM measurements in the Shumagin Islands segment (Figure 1b) of the subduction zone showed only a small amount of strain in the direction of relative plate motion, much lower than anticipated from locked subduction zone models [*Lisowski et al.*, 1988; *Savage and Lisowski*, 1986]. The Yakataga and Shumagin Islands segments were the only segments of the entire Alaska–Aleutian megathrust system that did not rupture in a great earthquake between 1938 and 1965, and there was a vigorous debate in the 1980s over whether the Shumagins segment represented a seismic gap that was

overdue for rupture, or a segment with low strain and unlikely to rupture in great earthquakes [*Boyd et al.*, 1988]. Vertical measurements in the Shumagins seemed to support the presence of subduction-related strain in that segment [*Beavan et al.*, 1984], although later and more precise measurements showed smaller or negligible vertical motions [*Beavan et al.*, 1986; *Hurst and Beavan*, 1987]. A later combination of EDM and GPS data showed that a small amount of horizontal contraction did occur across the Shumagin Islands, but only about 25% of what was expected from simple subduction zone models [*Larson and Lisowski* 1994; *Zheng et al.*, 1996].

1.2. Mobile Very Long Baseline Interferometry Measurements

A permanent very long baseline interferometry (VLBI) station was established in Fairbanks in the early 1980s, which operated until the end of 2005. In addition, mobile VLBI measurements were made at five sites in Alaska and one in Canada from 1984 to 1989, in order to study the Pacific–North America plate boundary. The most comprehensive summary of the velocities was presented by *Ma et al.* [1990]. The mobile VLBI data were also used to estimate displacements from the 1987–1988 Gulf of Alaska earthquake sequence, a series of earthquakes that occurred on a north–south trending feature on the Pacific plate south of the megathrust [*Argus and Lyzenga*, 1994; *Sauber et al.*, 1993].

The mobile VLBI data suffered from two significant drawbacks. The first was that most of the Alaska mobile VLBI campaigns contained very little data from sites outside of Alaska. As a result, the rotation of the network around the permanent Fairbanks point was poorly constrained, and as a result, the velocities of the sites differed considerably in different VLBI solutions (by as much as 3–4 mm/yr). However, the *Ma et al.* [1990] velocities compare quite well overall with the GPS velocity field, and orientation errors in that solution appear to be minimal. The main problem with the VLBI data was the small number of sites, which made interpretation of their velocities difficult. *Ma et al*. [1990] showed that the velocities of Kodiak and Cape Yakataga were generally consistent with the predictions of subduction zone models with a wide locked zone, whereas the velocity of Sand Point was intermediate between that expected for aseismic subduction and a locked subduction zone model. *Sauber et al.* [1993] compared the VLBI data from Cape Yakataga with the EDM line-length network, and found that these two data sets were compatible. The velocities for the interior sites were not easily explained. The mobile VLBI site at Whitehorse may have been unstable, because the VLBI velocity for this site is several mm/yr different from the velocity of the later GPS site WHIT.

1.3. GPS Measurements in Alaska

The first GPS measurements in Alaska date back to 1984, made by the National Geodetic Survey (NGS). Because the terrestrial geodetic network in Alaska was sparse and outdated, NGS carried out a series of statewide measurement campaigns from 1988 to 1991, aimed at providing a statewide High Accuracy Reference Network. Unfortunately, most of those campaigns came too early for the data to be useful for high-precision deformation measurements. Since then, NGS continued to carry out occasional surveys at airports and tide gauges, including some repeat measurements. The USGS carried out high-precision measurements in 1991 in the Shumagin Islands, and in 1992 in the ice fields near Yakutat, as final surveys of the old EDM networks. Much more extensive campaign GPS measurements were begun in 1993 by the USGS, Goddard Space Flight Center, and several universities, with three NASA-supported projects to study subduction-related processes in southern Alaska. Another important data set comes from the work of *Avé Lallemant and Oldow* [2000] in the western Aleutians, where data collection began in 1996.

We began to collect GPS data in many locations across Alaska in 1995, in several cases building on previous work done by other groups [e.g., *Cohen et al.*, 1995; *Sauber et al.*, 1997; *Savage et al.*, 1998]. We carried out numerous GPS campaign surveys throughout Alaska, which provided the bulk of the data used here. Although the continuous GPS site FAIR has operated since late 1991, no additional continuous sites were established until 1996, when the U.S. Coast Guard set up seven sites to support real-time navigation. Another 10 continuous sites were established from 1997 to 2002, and 16 more sites were set up shortly after the 2002 Denali Fault Earthquake to measure postseismic deformation. For the most part, GPS work in Alaska has been carried out through repeated campaign surveys. Today there are many more continuous sites, as the Plate Boundary Observatory has set up sites across all of Alaska, but these data were not used in the present compilation. This new network of continuous sites will usher in a new generation of GPS studies.

This paper summarizes research into Alaska active tectonics carried out over a roughly a decade and a half, using GPS geodesy. These observations (Table 1) provide a wealth of information about the active tectonic processes affecting the region. The earliest data used in this paper were collected in 1992, because the earlier data are difficult to place into the same reference frame as the modern data due to the weak global tracking network at the time. This paper presents and documents the contemporary deformation field, as determined from GPS site velocities at 78 sites using data spanning 1992–2002, and from 497 additional sites spanning

Table 1. Sources of Data Used in This Study

Source	Region	Time Span	Support
University of Alaska Fairbanks	All	1995–2007	NSF, NASA, USGS
US Geological Survey	Prince William Sound, Kodiak	1993–2000	NASA
Lamont-Doherty Earth Observatory	Alaska Peninsula	1993–1996	NASA
Goddard Space Flight Center	Chugach–St. Elias, Copper Basin, Kodiak	1993–2007	NASA
Rice University/University of Idaho	Aleutians	1996–1999	NSF
National Geodetic Survey	Airport Control Surveys	1994–1998	NGS/NOAA
National Ocean Service	Tide gauge surveys	2005–2006	NOS/NOAA
Alaska Dept. of Transportation	Denali fault crossing	1994	State of Alaska
Crazy Mountains Joint Venture	Denali Highway, road system	1994–2002	State of Alaska
R&M Consultants	All	2001	NGS/NOAA
LCMF, Inc.	Southern Coast, tide gauge surveys	2002–2006	NOS/NOAA

1992–2007 (575 total sites). Only sites located far enough from the rupture zone of the 2002 Denali Fault Earthquake [*Eberhart-Phillips et al.*, 2003] to have minimal effects from postseismic deformation [e.g., *Freed et al.*, 2006a, 2006b] are included in the second set, which is based on the solution used by *Cross and Freymueller* [2008]. Spatial and temporal subsets of this velocity field have been published previously [*Cohen and Freymueller*, 1997, 2004; *Cross and Freymueller*, 2007, 2008; *Fletcher*, 2002; *Fletcher and Freymueller*, 1999, 2003; *Fletcher et al.*, 2001; *Fournier and Freymueller*, 2007; *Freymueller and Beavan*, 1999; *Freymueller et al.*, 2000; *Larsen et al.*, 2004, 2005; *Mann and Freymueller*, 2003; *Ohta et al.*, 2006; *Sauber et al.*, 1997, 2006; *Savage et al.*, 1998, 1999; *Zweck et al.*, 2002], but the version presented here is the most complete and comprehensive, spanning the entire region and includes all usable data. In addition to data we collected, we incorporate data from GPS surveys collected by other academic groups, state and federal agencies, and by private land surveyors (Table 1). Surveys conducted for land surveying purposes often use much shorter observation times than those conducted for measurements of crustal deformation, so we normally used only surveys that lasted a minimum of ~5 h per day. Despite the lower precision, these surveys provide critical data in some areas. Compared to previous published results, we improved the individual solution quality by a systematic reanalysis of all data using consistent software and models, used a better and more accurate definition of the global and North America-fixed reference frames, and carefully rechecked field notes and logs to correct errors in antenna heights and antenna types. The result is the most precise and accurate three-dimensional (3-D) velocity field available for Alaska to date.

The 2002 Denali Fault Earthquake occurred during the time interval spanned by our velocity field. The earthquake caused significant displacements over a large area of southern and central Alaska [*Elliott et al.*, 2007; *Hreinsdóttir et al.*, 2006], and also triggered postseismic deformation over an area nearly as large [*Freed et al.*, 2006a, 2006b]. As a result, the use of post-earthquake data over significant areas of Alaska requires additional calibrations for the coseismic and postseismic offsets. The final day of data used in the pre-earthquake velocity solution (Table 2 and Table ES1 (Table ES1 found on the CDROM accompanying this volume)) is 19 October 2002, the day before the $M_w = 6.7$ Nenana Mountain Earthquake, the first major event in the 2002 Denali Fault Earthquake sequence [*Eberhart-Phillips et al.*, 2003]. For sites in the far field of the earthquake, we also include

Table 2. Summary of Solutions Used in This Study

Year	# Solutions	Notes
1992	65	May through July
1993	70	May through July
1994	65	June, July, late September
1995	121	May through October
1996	366	Start of continuous solutions
1997	365	
1998	365	
1999	365	
2000	366	
2001	365	
2002	288	Last day: 19 October 2002
2002	77	Only sites far from Denali fault
2003	365	
2004	366	
2005	365	
2006	365	
2007	284	Last day: 6 October 2007

post-earthquake data up through October 2007, corrected for the coseismic displacements predicted by the slip model of *Hreinsdóttir et al.* [2006].

2. DATA AND GPS DATA ANALYSIS

We have compiled the most complete GPS velocity field possible for both the pre-Denali earthquake period and the full study period. All data have been analyzed in a consistent manner using the same software and models, and combined into a single velocity solution to estimate site velocities. We divide the data analysis steps into three stages—GPS data analysis, reference frame, and velocity estimation—and describe each in order.

2.1. GPS Data Analysis

We analyzed all data presented in this paper using the GIPSY/OASIS GOA4 software developed at the Jet Propulsion Laboratory (JPL) [*Gregorius*, 1996; *Zumberge et al.*, 1997]. Beginning 1 January 1996, we analyzed and used every day of data from permanent GPS stations in and around Alaska and included all campaign stations. We did not analyze every day of data prior to 1996, but included all days with some campaign data. We then combined all of these daily GPS solutions into a single velocity solution to estimate linear velocities. In total, 2801 individual daily GPS solutions were used in the pre-earthquake velocity solution, and 4623 in the full solution (Table 2).

For data collected before 1995, we combined the data from Alaska with data from the global (IGS) network and estimated satellite orbits. In these solutions, we fit a satellite trajectory from existing orbit estimates (broadcast orbits, or a precise orbit), and integrated the equations of motion to generate an a priori orbit and associated partial derivatives for each satellite. We estimated the initial conditions (position and velocity) for each day's orbit, plus time-varying solar radiation pressure, along with station positions and other parameters. All site coordinates are estimated with loose constraints in our global solutions. For 1992 and 1993, we used every available GPS site around the world, no matter where it was located. By 1994, dense arrays of continuous GPS sites began to be deployed in Southern California and Japan, and the density of continuous sites in western Europe became higher than needed to determine orbit parameters, so for data from 1994 we use a well-distributed set of ~60 global stations in each daily solution. The exact stations used varied day-to-day based on data availability.

For data beginning in 1995, we combined data from Alaska with data from continuous GPS sites spanning North America, the Arctic regions of Eurasia, and a few additional sites in the central Pacific. The exact stations used varied day-to-day based on data availability. For these solutions, we fixed JPL's fiducial-free orbit (estimated without significant a priori site position constraints). This orbit is generated based on data from a global network of 50–85 stations, and because no station positions are constrained it is in no particular reference frame. However, the orbits are internally self-consistent, and the resulting solutions can be transformed into any reference frame by use of a seven-parameter similarity transformation.

We used both phase and pseudorange data from all sites (some receivers provided only phase data), and analysis models similar to those described by *Larson et al.* [1997] and *Freymueller et al.* [1999], although many models internal to the software have been updated since that time. We use network solutions rather than point positioning, and we normally used the site ALGO (Algonquin Park, Ontario, Canada) as a reference clock. When ALGO was unavailable or had clock or data problems, we used the site AMC2 (Colorado Springs, CO) as a reference clock. We applied elevation-dependent antenna phase center corrections based on the IGS_01 model, and applied the NOAA antenna calibrations (http://www.ngs.noaa.gov/ANTCAL/) for antennas not included in the IGS_01 model. We used all data from satellites 10° or more above the horizon, and estimated zenith wet tropospheric path delays using the Niell mapping function [*Niell*, 1996]. The a priori tropospheric path delay was set to an elevation-dependent value for the dry (hydrostatic) component, and 10 cm for the wet component, and we estimated a residual wet delay with azimuthal gradient. Finally, we applied an ocean tidal loading model calculated for each site based on the TPXO.2 ocean tidal model, using the SPOTL software [*Agnew*, 1997]. Ocean tidal loading amplitudes are very large for sites in southern Alaska, often in excess of 40 mm, due to the very large tidal range in the Gulf of Alaska. The even larger tidal range in Cook Inlet is not represented in any existing tidal model, and we see residual periodic errors (a strong fortnightly period) in our solutions consistent with aliasing of unmodeled ocean loading displacements [*Penna et al.*, 2007], especially for sites in that region.

2.2. Daily Reference Frame

We transformed each day's loosely constrained solution into the International Terrestrial Reference Frame 2000 (ITRF2000) reference frame, using the IGSb00 realization (reference URL given above), using ~20 reference frame sites to define the transformation. For each day, we compute the predicted position of each reference frame site based on the IGSb00 realization of ITRF2000 (using SINEX file ftp://igscb.jpl.nasa.gov/igscb/station/coord/IGS03P33_RS106.

SNX), and then compute the seven-parameter similarity transformation between our solution and the ITRF2000 prediction that minimizes the residuals at all reference frame sites. In computing the transformation, all sites present in both the solution and ITRF2000 are weighted based on the joint uncertainties in the ITRF and our solution. The typical 3-D weighted root-mean-square (WRMS) misfit after transformation is 4–6 mm for recent solutions, and the posttransformation 3-D WRMS residuals are usually ~15 mm for solutions in 1993 and ~20 mm for 1992. The WRMS values give a general idea of the precision with which the reference frame is defined on a daily basis.

We did not add uncertainty to the daily positions to account for uncertainties in the ITRF, because random daily errors in the realization of ITRF are most likely small compared to other uncertainties. However, there are significant uncertainties in the definition of the terrestrial reference frame that we account for by adding uncertainty to our estimated velocities. The most significant uncertainty in the definition of the ITRF is probably in the definition of the geocenter. It is well known that ITRF2000 and ITRF2005 have a geocenter *Z* rate difference of 1.8 mm/yr, and there are differences of similar magnitude between earlier versions of ITRF [*Argus*, 2007]. These differences make absolute plate rotations computed in ITRF specific to that version of ITRF, and for sites in Alaska they also affect the vertical velocities because a change in the definition of the geocenter affects the *Z* component of all site velocities, which maps more into the vertical than the horizontal for sites at high latitude.

2.3. Velocity Estimation and North American Frame

We used all daily GPS solutions in a linear network velocity estimation, to estimate positions at an epoch time (2000.0) plus velocities for the GPS sites (Figure 1). We present two solutions here, a pre-earthquake solution (1992–2002) and a 1992–2007 solution for sites far from the 2002 Denali fault earthquake, and we use the pre-earthquake solution only for sites not in the longer solution. The 1992–2007 solution is based on that used by *Cross and Freymueller* [2008]. In a few cases, colocated sites were assumed to have the same velocity, and only one velocity is presented here. Less than 10% of the sites in the solution are continuous GPS sites. We estimated only linear velocities with time, without periodic seasonal terms, since most sites are not continuous sites. The continuous GPS sites all have at least 5.5 years of data, so the velocities are unlikely to be biased by neglecting the seasonal terms, and all campaign surveys were done at nearly the same time of year (summer). All daily solutions were weighted according to the inverses of their covariance matrices resulting from the GIPSY analysis. We scaled the covariances of all solutions by a constant factor, 6.1 for the pre-earthquake solution and 8.9 for the 1992–2007 solution, based on the misfit to the velocity solution so that the χ^2 per degree of freedom of the velocity solution was equal to 1.0. This results in an increase in the uncertainties of all observations by a factor of 2.5–3. We would most likely have a slightly smaller scaling factor for the uncertainties if seasonal terms were estimated, because the continuous sites show significant seasonal variations (mostly in height) [*Freymueller*, in press]. However, almost all campaign surveys were carried out in the same 3- to 4-month period each year, so seasonal variations should have little effect on their site velocities. Master tables of all site velocities are given in Tables ES1 and ES2 (found on the CDROM accompanying this volume). All figures are based on this master site velocity table.

Velocities were then referred to the North American plate by subtracting the rotation of North America in ITRF from the ITRF2000 velocities. We use the recent determination of the motion of North America of *Sella et al.* [2007], which also used the IGSb00 realization of ITRF2000 and is thus the most consistent with our velocity reference frame. Using an older definition of North America, such as that of the REVEL 2000 model [*Sella et al.*, 2002], would change the horizontal site velocities relative to North America by 2–3 mm/yr. Experiments with different reference frame realizations show that this difference is almost entirely due to differences between ITRF97 (used for REVEL) and ITRF2000/IGSb00 (used by *Sella et al.* [2007]). The most significant difference between the frames is in the geocenter rate. The recent SNARF 1.0 realization of a North America-fixed reference frame (http://www.unavco.org/research_science/workinggroups_projects/snarf/snarf.html) predicts motions that differ by about 1 mm/yr from those of *Sella et al.* [2007]. This difference between the two recent studies results from the use of a different site distribution to define stable North America and a different strategy to account for Glacial Isostatic Adjustment across northern North America. Differences between predicted velocities are much smaller in the lower 48 states of the United States, but are amplified in Alaska by the large distance to the stable part of North America. This difference may be indicative of the level of uncertainty in the definition of the North American frame.

The uncertainties in ITRF and the North American frame discussed above are much larger than the random errors in site velocities for many sites, including most of the campaign sites with long measurement histories. We thus augment the covariance matrix of the velocities to account for both elements of the reference frame uncertainty. The first component of uncertainty is in the *Z* component, where we add 1.8 mm/yr uncertainty to all sites based on the difference

between ITRF2000 and ITRF2005. This uncertainty is perfectly correlated from site to site, so that it affects only absolute velocities and not relative velocities. At 60°N, this maps into an additional uncertainty of 1.6 mm/yr in the local vertical, and 0.9 mm/yr in the north component, added in quadrature to the uncertainty from random error. We also add an uncertainty in the North American plate rotation equal to the difference between the angular velocities of *Sella et al.* [2007] and SNARF 1.0. The difference between these two is equivalent to a rotation about a pole located near Mobile, AL. For sites in Alaska, this amounts to an additional uncertainty of ~1 mm/yr, with an elongate error ellipse oriented NW–SE. Because we propagate these uncertainties using the full covariance matrix, this uncertainty is also highly correlated for nearby sites and has a limited effect on relative site velocities.

3. OBSERVED SITE VELOCITIES

The estimated site velocities (Figures 2–12) show substantial spatial variation, resulting from a variety of active tectonic and volcanic processes. These include elastic strain resulting from the slip deficit of the locked subduction zone, which varies along strike, postseismic deformation following the 1964 earthquake, glacial isostatic adjustment from the post-Little Ice Age (LIA) ice melting, the relative motion of large tectonic blocks making up part of the crust of Alaska, and inflation of active volcanoes.

Each of the subsections below discusses the observed velocities for a region of Alaska. We highlight the most important features of the data, based on the published papers that used it. More extensive discussion of models to explain the data in some of these regions will be presented in a later section; in this work we present the observations and summarize the main contributions to the velocities. Because of the large variations in the density of sites and magnitude of velocities, map scale and velocity scales differ for each figure. As the discussion for each of these regions necessarily uses local place names, we encourage the reader to refer to the regional maps.

3.1. Southeast Alaska

Southeast Alaska undergoes extraordinary uplift due to glacial isostatic adjustment from the rapid melting of glaciers and ice fields that followed the LIA. The LIA glaciation in southern Alaska reached its peak ~1900 A.D., although deglaciation in some regions began up to a century earlier [*Calkin et al.*, 2001; *Motyka*, 2003; *Wiles et al.*, 1999]. Peak uplift rates in the region exceed 30 mm/yr, and most sites along the coast and coastal mountain belt uplift at rates exceeding 10 mm/yr (detailed later in section 3.7). *Larsen et al.* [2004, 2005] showed that this rapid uplift can be explained using the known ice load history with an elastic crust about 60 km thick overlying a low-viscosity asthenosphere. Horizontal motions from glacial isostatic adjustment cause radial extension centered on Glacier Bay, and may cause horizontal motions larger than 5 mm/yr in some cases (Elliott et al., in preparation), although this effect is not considered in this paper.

The Fairweather fault is the most active part of the Pacific–North America plate boundary in Southeast Alaska (Figure 2; *Plafker et al*. [1978]). The Fairweather fault is the onshore extension of the offshore Queen Charlotte transform fault to the south, and it terminates in a complex transition with the Chugach–St. Elias fault in the north. Pacific–North America plate motion is roughly parallel to the Queen Charlotte fault, but the strike of the Fairweather fault (N34°W) is rotated clockwise by 23° relative to the Pacific–North America convergence direction (N11°W); this requires significant deformation to occur on other faults because the motion on the Fairweather fault is strike slip. A splay of the Fairweather fault may extend further to the northwest, to connect with the Totschunda and Denali faults, as originally proposed by *Richter and Matson* [1971], although no such fault has yet been mapped. The Denali fault lies ~100 km inboard of the Fairweather fault in this region, and Quaternary offsets of the Denali fault have been documented at several locations [*Matmon et al.*, 2006; *Plafker et al.*, 1994], although evidence for activity along its southern extension, the Chatham Strait fault, is lacking.

Right-lateral shear on the Fairweather fault dominates the GPS velocity field for this region. The site in Yakutat (YKTT) on the Pacific coast moves 45 mm/yr toward N30°W relative to Whitehorse (WHIT), located ~300 km inland. This relative motion vector is within 4° of being parallel to the strike of the Fairweather fault (N34°W). Velocities of all other sites along the Pacific coast are also very close to parallel to the Fairweather fault, indicating that right-lateral strike-slip motion parallel to the Fairweather fault is the dominant tectonic motion. *Fletcher and Freymueller* [1999, 2003] interpreted this direction of motion to indicate that the Yakutat terrane moves (relative to North America) parallel to the Fairweather fault, rather than in the direction of the Pacific plate as had been suggested earlier [e.g., *Lundgren et al.*, 1995].

Lisowski et al. [1987] estimated the slip rate of the Fairweather fault to be 41–51 mm/yr based on repeated line-length measurements of a dense network across the fault near Yakutat. The wide range of possible slip rates resulted from a strong tradeoff between the fault slip rate and locking depth; any locking depth ≥4 km could fit the data equally well, with lower slip rates associated with shallower locking

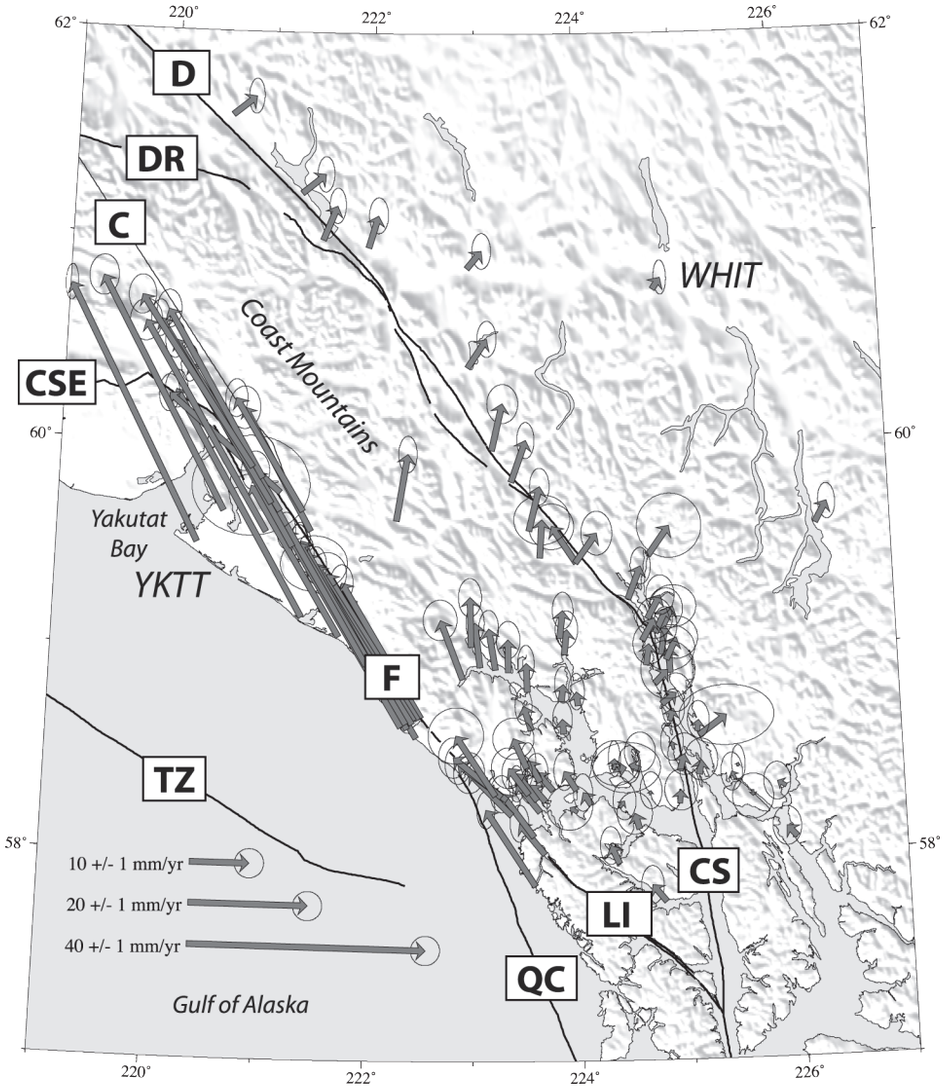

Figure 2. Horizontal velocities from southeast Alaska. The sites Whitehorse (WHIT) and Yakutat (YKTT) are labeled. Major faults are shown in black and marked with letters inside boxes: D, eastern Denali Fault; DR, Duke River Fault; C, Connector Fault; CSE, Chugach–St. Elias Fault; F, Fairweather Fault (almost entirely covered by green arrows); TZ, Transition Zone; QC, Queen Charlotte Fault; LI, Lisianski Inlet–Peril Strait Fault; CS, Chatham Strait Fault.

depths. This is a defect of the network, because all sites were located within 10 km the fault. Several sites from that network have been surveyed repeatedly using GPS, and *Fletcher and Freymueller* [2003] modeled these GPS velocities and EDM line length changes and estimated the best-fitting slip rates on the Fairweather and eastern Denali faults to be 45.6 ± 2.0 and 3.8 ± 1.4 mm/yr, respectively, with a locking depth of 9.0 ± 0.8 km for the Fairweather fault.

Similar Fairweather-parallel motion persists to the west of this region, for coastal sites on the south side of the St. Elias Range, almost as far west as Prince William Sound (Figure 3). However, the coastal sites on the south side of the St. Elias Range move at a slower rate than the sites from Yakutat to the south, which may indicate that active convergent structures in the St. Elias Range extend nearly as far southeast as Yakutat Bay. This is consistent with the EDM

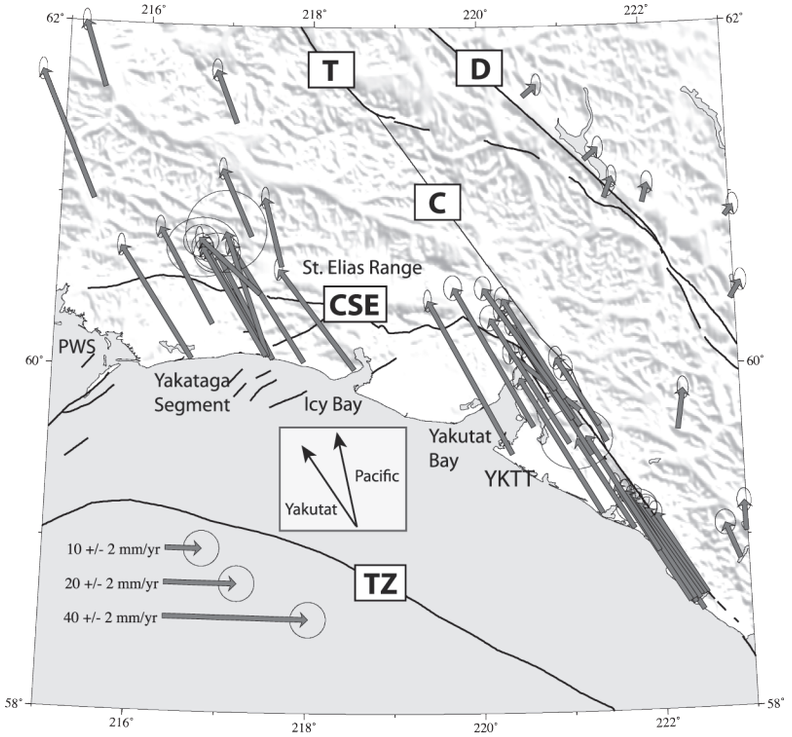

Figure 3. Horizontal velocities from southeast Alaska and the St. Elias region. Major faults are shown in black and marked with letters inside boxes: D, Denali Fault; T, Totschunda Fault; C, Connector Fault; CSE, Chugach–St. Elias Fault; TZ, Transition Zone. Inset shows the Pacific–North America and Yakutat–North America relative motion directions. The site YKTT is labeled.

data from the 1980s, which showed the strain tensor in the region to be dominated by contraction in the N32°W ± 2.4° direction [*Savage and Lisowski*, 1988], which is parallel to the Fairweather fault and the GPS velocities. *Sauber et al.* [1997] modeled one component (Pacific-parallel direction) of the velocities across the St. Elias Range using a subduction model with deformation caused by the subducting Pacific plate. Although their model fit the one component modeled well, it failed to explain the orientation of the observed velocity vectors. However, a very similar model in which the subducting plate is the Yakutat terrane, moving in a Fairweather-parallel direction, provides a good first-order fit to the data [*Elliott et al.*, 2006].

Inland sites show an east to northeast-directed motion relative to North America (Figures 2 and 3). Much of this can be explained by glacial isostatic adjustment (Elliott et al., in preparation), but the remainder may be caused either by an error in the definition of stable North America or by NE-directed motion of the northern Canadian Cordillera, as suggested by *Mazzotti and Hyndman* [2002]. The increasing velocity to the north observed for the inland sites is consistent with the latter explanation.

3.2. South-Central Alaska

Site velocities across South-central Alaska are spatially complex, showing the influence of several significant contributions to the deformation field (Figure 4). From east to west, velocities of coastal sites rotate systematically from a Fairweather-parallel orientation in the St. Elias Range east of Prince William Sound (see also Figure 3) to a Pacific-parallel direction in the eastern Kenai Peninsula (Figure 4). This rotation of velocities must result from a transition in the subducting plate from the Yakutat terrane in the east to the Pacific plate in the west. Beneath Prince William Sound, the North American plate, Yakutat terrane, and Pacific plate form a three-plate "sandwich," with the Yakutat terrane in the middle. The Pacific plate underthrusts the Yakutat terrane at the eastern end of the Alaska–Aleutian trench, and the Yakutat terrane underthrusts North America [*Brocher et*

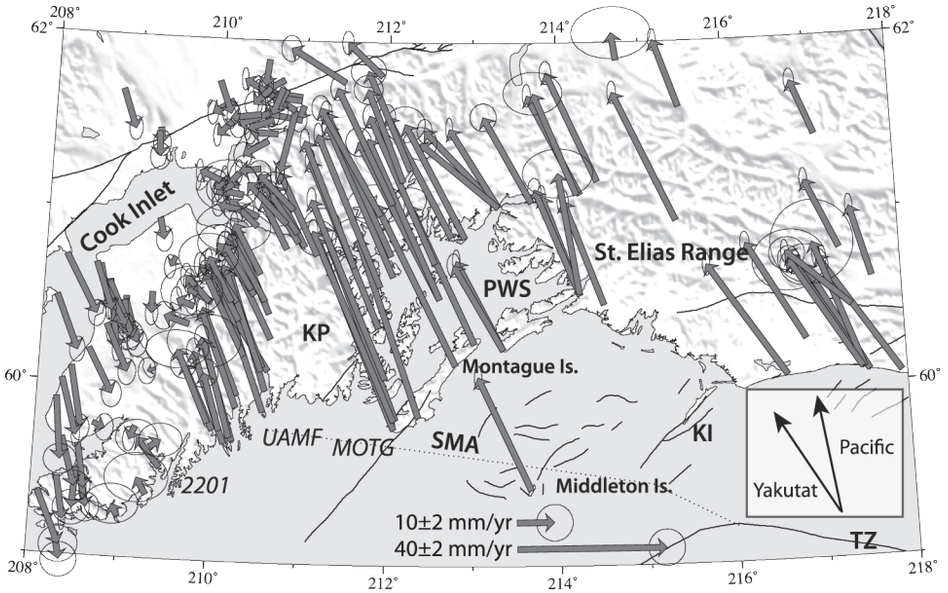

Figure 4. Horizontal velocities from Prince William Sound, the Kenai Peninsula, and Upper Cook Inlet. The shaded area is the rupture zone of the 1964 earthquake, and the star is its epicenter. Important geographic features are labeled: KP, Kenai Peninsula; PWS, Prince William Sound, KI, Kayak Island. Sites referred to in the text are labeled in italics. The inset shows the Pacific–North America and Yakutat–North America relative motion directions. The light dotted line offshore south of Montague Island shows the location of the Slope Magnetic Anomaly (SMA), considered to represent the southwest edge of the subducted Yakutat terrane crust. TZ, transition zone.

al., 1994; *Fuis et al*., 2008]. This three-plate system makes a transition westward to normal subduction of the Pacific plate as the Yakutat terrane pinches out. The southwestern limit of the Yakutat terrane in the subsurface has generally been inferred to be the Slope Magnetic Anomaly, which extends from the Transition Zone to the SW edge of Montague Island [*Griscom and Sauer*, 1990]. *Von Huene et al*. [1999] proposed that the edge of the Yakutat terrane in the subsurface and the edge of the Prince William Sound asperity of the 1964 Alaska earthquake coincide. *Brocher et al.* [1994] suggested that the Prince William Sound asperity lies between the Yakutat terrane and North America, not between the Pacific slab and North America. This question will be revisited in section 4.4.

Across the Kenai Peninsula, the magnitude of coastal site velocities drops dramatically with distance west from Prince William Sound, from 56 mm/yr at Montague Island (MOTG) to 35 mm/yr at Seward (UAMF), to 10 mm/yr at Nuka Bay (2201). Further west, the velocities reverse orientation and become trench-normal. Inland, a similar pattern is found, although sites with trenchward velocities are found throughout the Cook Inlet region. The regions of landward (Pacific-parallel) and trenchward velocities roughly correspond to the mountainous and lowland regions of the Kenai Peninsula, but at the SW end of the Peninsula even sites in the Kenai Mountains move toward the trench. The average orientations of the two sets of velocities are nearly opposite to each other. Between the two groups lie several sites with near-zero velocities, and most of these site velocities are deflected to the west.

Savage et al. [1998] presented the first quantitative deformation model for this region, based on relative velocities within a profile at the western edge of Prince William Sound, observed from 1993 to 1997. This profile did not show the trenchward motion, and they explained the velocities using a 2-D (uniform in the along-strike direction) dislocation model with the plate interface dipping 3° to the NNW. Although they obtained a reasonable fit to the data, the deformation across their network could not be matched unless they assumed the plate convergence rate to be ~20% faster than the long-term plate convergence rate. They inferred that the additional strain resulted from continuing postseismic relaxation.

Freymueller et al. [2000] explained the complexity of the deformation field as resulting mainly from the superposition of two major components: postseismic deformation after the

1964 earthquake (trenchward motion), and elastic deformation from the shallow locked part of the megathrust. The latter component shows significant along-strike variations, caused by a contrast between the wide locked zone beneath and south of Prince William Sound and the eastern Kenai Peninsula with a narrow or nonexistent locked zone beneath and south of the western Kenai Peninsula. Where the elastic signal is smaller or missing, the trenchward velocities extend closer to the trench. Where the elastic signal is large, such as in the Prince William Sound area, velocities in the direction of the Pacific–North America relative motion extend much further inland. Where these two components cancel, the remaining westward motion of sites may indicate a westward tectonic escape of material away from the colliding Yakutat terrane.

The pattern of vertical velocities (Plate 1) agrees with the general predictions of the classic subduction zone model [*Savage*, 1983], with subsidence found near the coast and offshore, and uplift found inland. A possible second region of subsidence is observed NW of Upper Cook Inlet. The amplitudes of vertical velocities are substantial, with the highest subsidence rates being observed on the Pacific coast of the Kenai Peninsula, seaward of Seward, and across Prince William Sound. There are two nearly separate regions of subsidence along the coast, one in Prince William Sound and the other on the coastal Kenai Peninsula, separated by a zone of essentially zero vertical motion that passes through the SW end of Montague Island. Middleton Island, well offshore, shows extremely rapid uplift, as noted by *Savage et al.* [1998]. Middleton Island shows geological evidence for long-term uplift, including a series of uplifted marine terraces [*Plafker et al.*, 1992].

3.3. Interior Alaska and the Denali Fault

There is abundant seismicity north of the Denali fault, with dense clusters of microseismicity in the Fairbanks area (Figure 5), and a diffuse band that extends north to the Arctic Ocean [*Ruppert et al.*, this volume]. Some of these earthquakes occur just north of the Denali fault on faults that parallel the Denali, and others may occur on faults that make up a foreland fold-and-thrust belt at the northern edge of the Alaska Range [*Bemis*, 2004; *Bemis and Wallace*, 2007; *Lesh and Ridgway*, 2007]. Most, however, occur on a series of NNE-trending strike-slip faults that extend well to the north of the Alaska Range [*Page et al.*, 1995]. Focal mechanisms for the larger earthquakes on these faults show left-lateral strike-slip motion [*Ruppert et al.*, this volume]. The Kantishna cluster, the region of the most abundant microseismicity in Alaska, is located where one of the NNE-trending zones intersects the fold belt. Seismicity in the Kantishna cluster includes earthquakes on structures parallel to the Denali fault as well as NNE-trending structures [*Burris*, 2007].

Velocities of sites in the Alaska Range and Interior Alaska to the north (Figure 5) are much slower than those of sites on the southern coast. North of the Alaska Range, site velocities are almost all <5 mm/yr, excluding sites with large uncertainties. Most well-determined sites move southward or southeastward relative to North America, and vertical velocities are generally not significantly different from zero. South of the Alaska Range the pattern of velocities is more complex. In the west, near Talkeetna, sites move rapidly to the south–southeast, toward the trench, continuing the pattern observed in Cook Inlet. In the east, however, site velocities are away from the trench, more consistent with the expectations from a locked subduction zone model. A rotational component of the velocity field is clearly visible in the velocities of sites near the Denali fault. The trace of the Denali Fault curves significantly over this region, and velocities of sites near the fault rotate to remain nearly fault-parallel. This is particularly notable in the velocities of sites within 50 km south of the Denali fault, such as FCRK, PAXS, SOUR, and 7297, and sites to the west of them.

Southwest of this region, the velocity field includes a component of trenchward motion, like the sites in the Cook Inlet region. However, near the Denali fault, relative velocities show almost pure fault-parallel right-lateral shear. Figure 6 shows velocities relative to the continuous site GRNR (Healy). Velocities relative to GRNR on the main fault-normal profile are almost purely fault-parallel, and increase by 8 mm/yr across the Alaska Range in a right-lateral sense. The site DFLY moves ~3 mm/yr westward relative to GRNR, and sites south of DFLY show similar velocities; sites south of the active strand of the Denali fault (PISA, SSWB, R109, M110, DH97) show faster westward motion. *Fletcher* [2002] interpreted this pattern as evidence for two active fault strands in the Denali fault system, one between GRNR and DFLY and one at the McKinley strand. The edge of the region of trenchward velocities appears to be sharp, as there is a large difference in velocities between WOND at Wonder Lake, and the remaining sites ~100 km to the east. WOND shows a southward component of ~7 mm/yr relative to sites due east of it. An alternative explanation for the southward motion of WOND involves it being located on the Bering plate (see section 6). Similarly, the site HURR south of the Alaska Range includes a significant trenchward component in addition to its Denali fault-parallel component of motion.

Horizontal and vertical velocities along a fault-normal profile at longitude 146°W reveal an intriguing observation (Figure 7). The fault-parallel velocities increase by 6 mm/yr

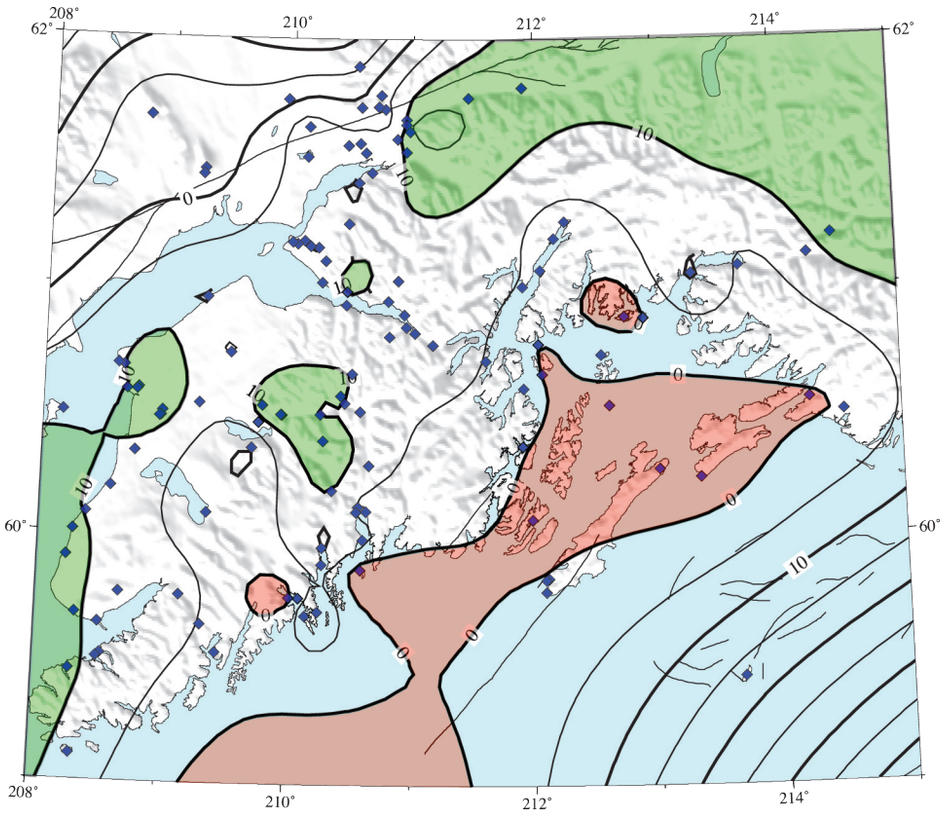

Plate 1. Contoured vertical velocities (1992–2007) from Prince William Sound, the Kenai Peninsula, and Upper Cook Inlet, in mm/yr. Red shaded regions are regions of subsidence, whereas green shaded regions have uplift rates in excess of 10 mm/yr.

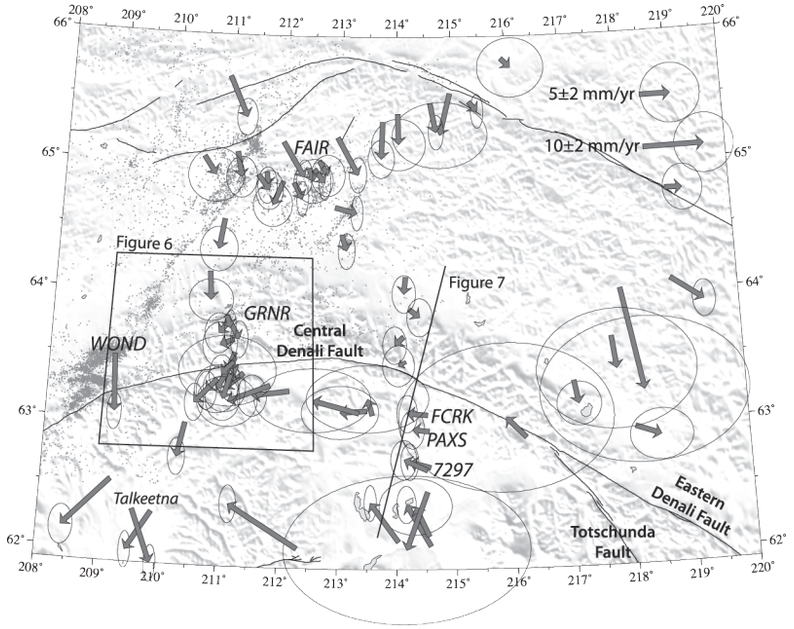

Figure 5. Horizontal velocities from Interior Alaska. Sites referenced in the text are labeled in italics, and important faults are shown in black and labeled. Gray dots are relocated earthquake epicenters from *Ruppert et al*. [this volume], most of which align into NNE-trending lineaments. The Kantishna cluster is the prominent cluster of seismicity at the west edge of the figure, near the site WOND. The box shows the location of Figure 6, and the line show the location of the profile shown in Figure 7.

along this profile. But vertical velocities change by about the same amount across the Denali fault, with the south side uplifting ~6 mm/yr relative to the north side. The change in the vertical velocities occurs within a ~40-km-wide zone across the fault, in which we have no data. Although this change is roughly coincident with the Denali fault, it is not likely that this reflects a significant vertical slip rate on the fault. During the 2002 Denali Fault Earthquake, vertical surface offsets were consistently north-side up, and averaged less than 13% of the horizontal motions [*Haeussler et al.*, 2004]. Geodetic slip models confirm that a dominantly strike-slip mechanism characterized the earthquake rupture at all depths [*Elliott et al.*, 2007; *Hreinsdóttir et al.*, 2006]. If the same ratio of vertical to horizontal motion applies to the interseismic period, this might account for ~1 mm/yr of vertical motion across the fault. The vertical velocity contrast might be related to interseismic strain on thrust faults that parallel the Denali fault, but if so then these faults would have to produce large vertical motions without significant fault-normal contraction; although possible, this seems unlikely. The vertical velocity contrast might reflect the combined effects of far-field deformation associated with subduction/collision in the south, plus uplift associated with the draining of glacial Lake Ahtna, which filled much of the present Copper River Basin. Few studies of Lake Ahtna have been published, but basic findings are summarized by *Péwé* [1975]. The lake filled much of the current Copper River basin, and narrow branches of the lake extended north nearly to the Alaska Range. It is not clear whether this mechanism can produce such a steep gradient in vertical velocities. The cause of this change remains a mystery to be addressed by future studies.

3.4. Alaska Peninsula

Velocities of sites along the length of the Alaska Peninsula show dramatic along-strike variations (Figure 8). In the northeast, in the Kodiak and Semidi segments of the subduction zone, the velocities show significant contraction in the direction of Pacific–North America plate motion, and sites on the Pacific side of the peninsula all move in the direction of Pacific–North America relative plate motion. Velocities are much slower in the Shumagin segment, but data are much sparser. *Larson and Lisowski* [1994] used EDM data and very early GPS data to show that contraction across the Shumagin Islands was small, only 4 ± 2 mm/yr, and much slower than expected for a locked subduction zone model.

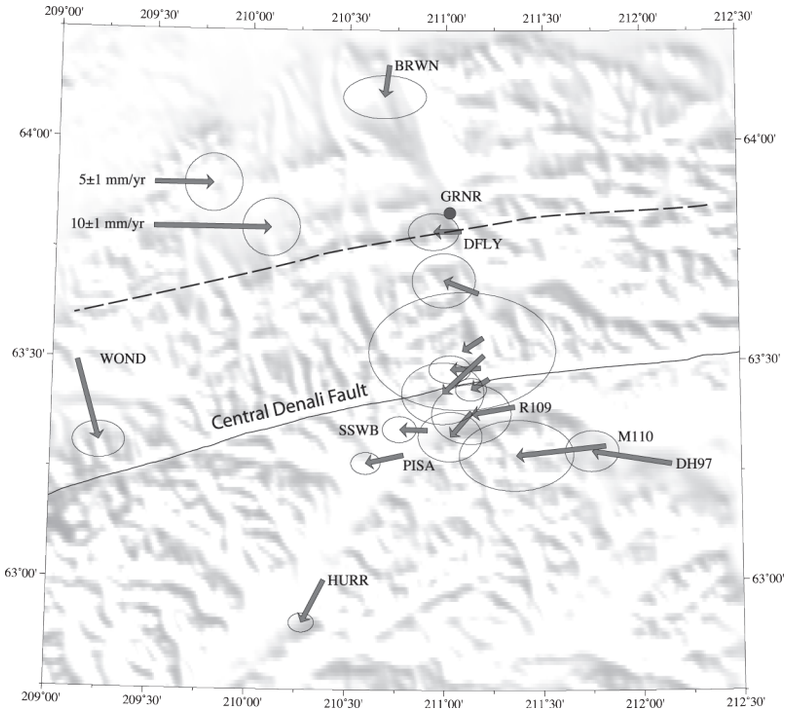

Figure 6. Horizontal velocities across the Alaska Range, relative to GRNR (large dot). The trace of the Denali fault is shown with a thick line. The central Denali fault is labeled, and the dashed line shows the approximate location of a northern fault strand inferred by *Fletcher* [2002].

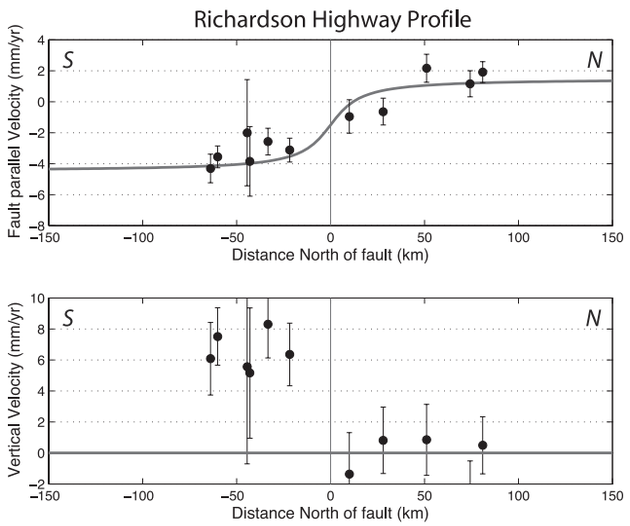

Figure 7. Denali fault profile along the line shown in Figure 5. (top) Horizontal velocities. Model curve is for an infinite strike-slip fault in an elastic half-space, with a slip rate of 6 mm/yr and a locking depth of 12 km. This model assumes that the sites north of the fault move 1.5 mm/yr eastward relative to North America due to continuing postseismic deformation from the 1964 earthquake (see section 4.1). (bottom) Vertical velocities. Sites south of the fault show a systematic uplift rate of ~6 mm/yr relative to the sites on the south side.

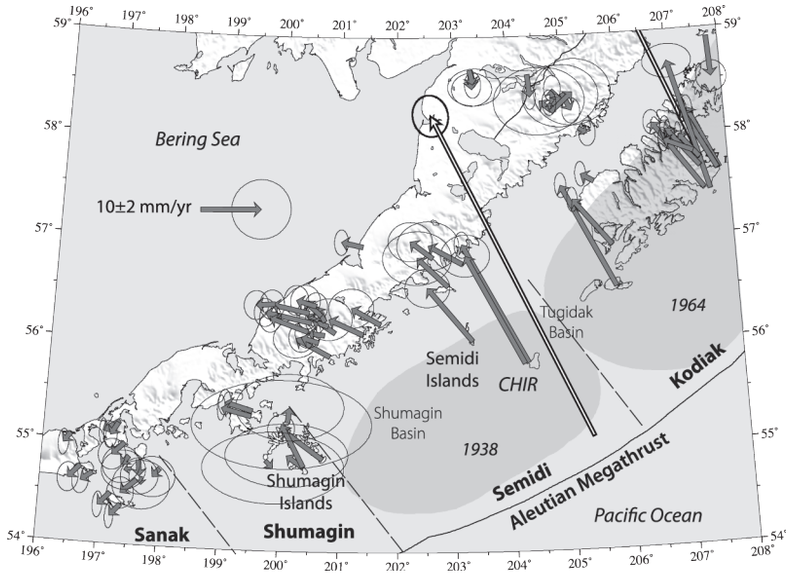

Figure 8. Horizontal velocities from the Alaska Peninsula. The white vector outlined in black is the Pacific–North America relative motion vector. Subduction zone segments are labeled and separated by dashed lines, and the shaded areas represent the rupture zones of the 1938 and 1964 earthquakes. The location of site CHIR on Chirikof Island is shown as well.

This is consistent with our results. Finally, at the SW end of the Alaska Peninsula, velocities are nearly trench-parallel and there is no indication of any contraction in the direction of relative plate motion.

Fournier and Freymueller [2007] explained the variations in contraction in terms of along-strike changes in plate coupling. Along the trench-normal profile of sites in the Semidi segment, there is a significant rotation of the velocities; with sites farther from the trench having velocities oriented significantly more westward than sites closer to the trench. Chirikof Island moves 37.3 ± 0.7 mm/yr toward N28 ± 1°W. Sites along the Pacific coast move 11 ± 2 mm/yr, but oriented toward ~N65°W. *Fournier and Freymueller* [2007] showed that this rotation can be explained by the superposition of contraction in the direction of plate motion with an overall south to southwestward translation of the region. *Cross and Freymueller* [2008] argued that this translation is best explained by the Alaska Peninsula lying on a separate and rigid Bering plate, which rotates clockwise relative to North America about a pole located in east Asia [*Fujita et al.*, 2002; *Mackey et al.*, 1997].

3.5. Western Alaska, the Bering Sea, and the Eastern Aleutians

There are only a few sites with velocities from western Alaska. Sites on the Bering Sea coast in western Alaska and the Bering Sea islands (Figure 9) show southward to south–southwestward velocities of ~5 mm/yr. Sites inland of the Bering Sea coast, in the central part of western Alaska, however, show a southeastward motion of ~10 mm/yr, similar to the trenchward motion seen in Cook Inlet. This southeastward motion mainly appears to affect sites located downdip of the 1964 earthquake, and is likely to be due to postseismic deformation after the 1964 earthquake (Suito and Freymueller, submitted manuscript, 2008). *Cross and Freymueller* [2008] showed that the motion of the Bering Sea sites is consistent with the clockwise rotation of a rigid Bering plate about a pole located in east Asia. The motion of the site SPSW on St. Paul Island, the southernmost of the Bering Sea sites (Figure 9), is similar to the velocities in the Sanak segment of the Alaska Peninsula, also consistent with a rigid Bering plate.

Most sites in the eastern Aleutians are located on active volcanoes, and show substantial and time-variable deformation. These sites are not considered here, because they are not amenable to being described in terms of constant velocities. Volcanic deformation at Okmok Volcano (Figure 10) amounts to up to half a meter of displacement, with much of that occurring in two main pulses of inflation in 2002–2003 and 2004 [*Lu et al.*, 2000a, 2005; *Miyagi et al.*, 2004; *Fournier and Freymueller*, 2007; T. Fournier, J. T. Freymueller, and P. Cervelli, Tracking magma volume recovery at Okmok Volcano using GPS and an Unscented Kalman Fil-

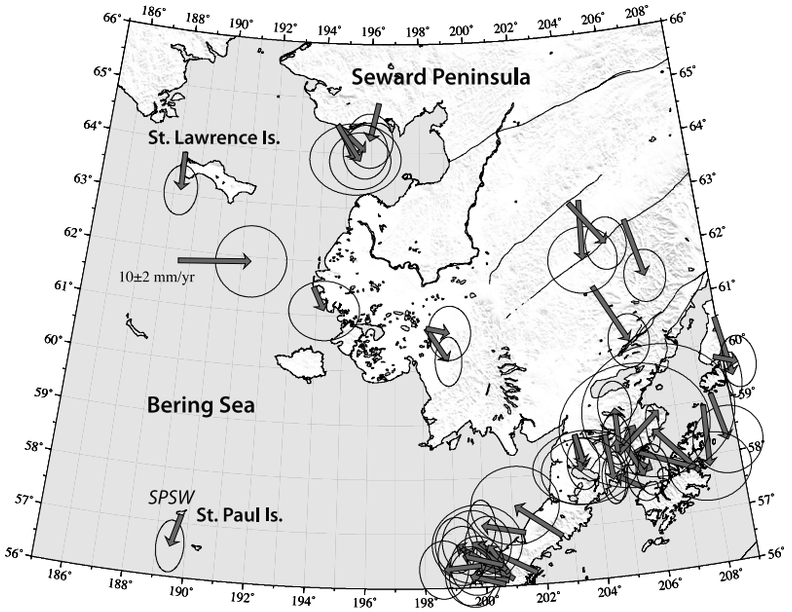

Figure 9. Horizontal velocities from Western Alaska. Sites on the Bering Sea islands and in western Alaska move southward to southwestward, showing rotation of the Bering plate relative to North America [*Cross and Freymueller*, 2008].

ter, submitted to *J. Geophys. Res*., 2008, hereinafter referred to as Fournier et al., submitted manuscript, 2008]. Deformation at Akutan Volcano is primarily related to the injection of a large dike in 1996, and its aftereffects [*Lu et al.*, 2000c]. Significant volcanic deformation has also been detected on Westdahl volcano at the western end of Unimak Island [*Lu et al.*, 2000b; *Mann and Freymueller*, 2003]. A few GPS sites on Akutan, in Dutch Harbor, and on Umnak Island to the west are not significantly affected by volcanic deformation. Away from active volcanoes, velocities of sites in the eastern Aleutian arc are dominantly trench-parallel, with a small and variable component of strain in the direction of relative plate motion.

3.6. Central and Western Aleutian Arc

As in other segments of the Aleutian subduction zone, sites in the central and western Aleutians show evidence for along-strike variations in strain in the direction of plate motion, indicative of variations in plate coupling. For example, in the Andreanof Islands segment, sites on Atka move ~5 mm/yr to the southwest, whereas sites on Adak and Kanaga islands move 10–15 mm/yr to the northwest (Figure 10). This region was studied in detail by *Cross and Freymueller* [2007], who concluded that the plate interface offshore of Adak and Kanaga islands was locked over a wide area, whereas that in the Atka region was dominantly creeping. This large along-strike change in slip deficit explains the contrast in the observed velocities.

However, sites from Amchitka to the west show an additional component of arc-parallel translation, relative to sites east of Amchitka (compare Figures 10 and 11). The site BKEB on eastern Amchitka moves 20 mm/yr in a nearly westward direction, whereas sites in the Near Islands (Attu and Shemya) move more than 30 mm/yr in a largely trench-parallel direction, and the site BKI on Bering Island in the Russian Komandorsky Islands moves more than 50 mm/yr in a largely trench-parallel direction [*Gordeev et al*., 2001]. *Cross and Freymueller* [2008] showed that these velocities require a significant component of motion on strike-slip faults north of the arc due to slip partitioning of oblique subduction, so that the western Aleutian arc now moves westward as a sliver or series of slivers. This is consistent with ideas based on the geology of arc basins [*Geist et al.*, 1988].

3.7. Vertical Motions

Vertical motions over much of Alaska are significant, because of its location on a convergent plate boundary, and because of postseismic vertical motions from the large megathrust earthquakes. However, the most rapid uplift does not occur along the subduction boundary, but in southeast Alaska, and has a nontectonic origin. Rapid uplift due to unloading—caused by the melting of glaciers and ice fields—extends

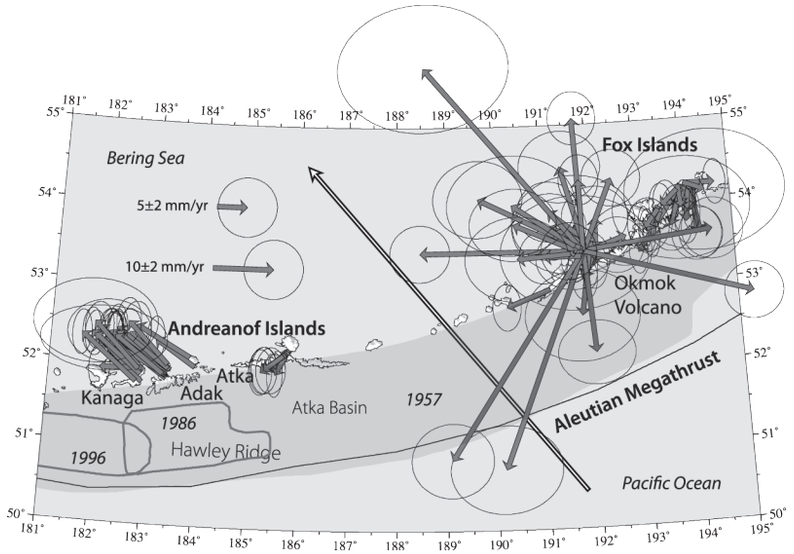

Figure 10. Horizontal velocities of selected sites from the eastern and central Aleutian arc. The white vector shows the Pacific–North America relative plate motion. The large radial-outward velocities in the eastern part of the figure result from inflation of Okmok volcano [*Miyagi et al.*, 2004; Fournier et al., submitted manuscript, 2008]. The shaded area is the rupture zone of the 1957 earthquake, and the rupture areas of the 1986 and 1996 earthquakes are outlined. The locations of the Atka Basin and Hawley Ridge are labeled.

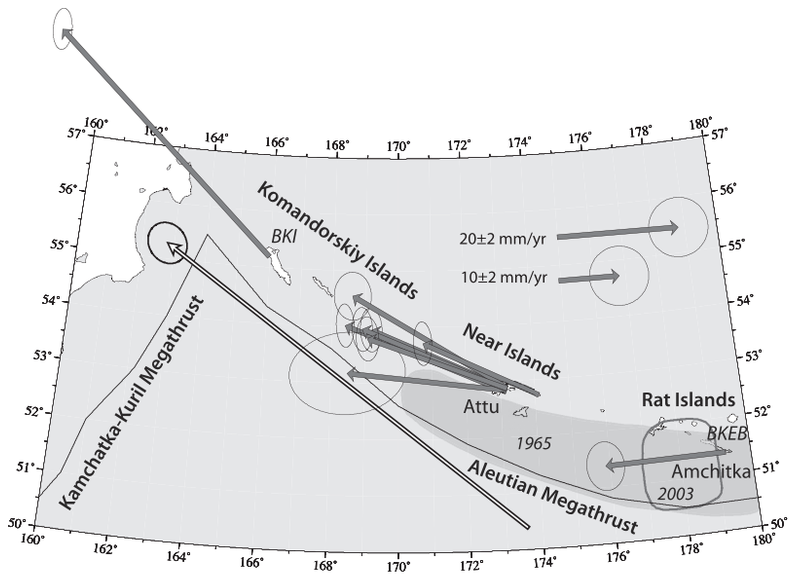

Figure 11. Horizontal velocities from the western Aleutian arc. The shaded area is the aftershock zone of the 1965 earthquake, and the aftershock zone of the 2003 earthquake is outlined. Sites referenced in the text are labeled in italics. The white vector is the Pacific–North America relative plate motion, which is nearly trench-parallel in the westernmost part of the arc.

across southeast Alaska and much of the southern coast of Alaska. This uplift can be explained in terms of the known glacial unloading history, and a reasonable viscoelastic earth model [*Larsen et al.*, 2005].

Uplift across northern SE Alaska exceeds 10 mm/yr over a broad region (Figure 12). There are two main peaks in the uplift rates, where they exceed 30 mm/yr, centered on Glacier Bay and the ice fields above Yakutat. The uplift in Glacier Bay is dominated by the viscoelastic relaxation caused by the deglaciation of Glacier Bay from ~1750 to 1900, whereas the uplift in the mountains northeast of Yakutat is dominated by the loss of ice over the last century [*Larsen et al.*, 2005].

Vertical motions in Alaska are not steady in time, but include a large seasonal component. Figure 13 shows the time series of vertical positions of site GUS2 in Gustavus, which has operated continuously since early 1997. The long-term trend is uplift, with the average uplift rate being 20.0 ± 1.5 mm/yr. Superimposed on this trend is an annual cycle with a peak-to-peak amplitude of ~17 mm, nearly equal to the average annual rate. The annual signal is not purely sinusoidal, featuring a broad peak of high positions in the summer, and a narrower trough of low positions in the winter [*Freymueller*, in press]. The site begins to uplift in April, roughly coinciding with the beginning of significant runoff from spring melt, and begins to subside in November, roughly coinciding with the beginning of substantial winter snow accumulation. All continuous GPS sites in Alaska show a similar pattern of seasonal motions, which is consistent with snow loading as the principal cause, a mechanism *Heki* [2003] proposed for northern Japan, and *Grapenthin et al.* [2006] proposed for Iceland.

4. SEISMIC CYCLE AND TECTONIC MODELS

The preceding section showed regional views of the velocity field, summarized the first-order features of the data and of a number of previous published papers, and highlighted the main conclusions of those papers. This section discusses seismic cycle and tectonic models in more detail. The spatially and temporally complex pattern of crustal deformation in Alaska results from several sources, which are often not easy to unravel. In several regions, a complex velocity field can be explained in terms of a superposition of two main sources [*Cross and Freymueller*, 2007; *Fournier and Freymueller*, 2007; *Freymueller et al.*, 2000]. However, in other regions there are three or more significant sources, or temporal variations, and some of these remain the topic of ongoing work. For example, the velocities shown here average across the time of the 1998–2001 slow-slip event (SSE) in Cook Inlet. Although the total displacements caused by the SSE have been measured and modeled [*Ohta et al.*, 2006], the time history has been more difficult to unravel because of the small number of continuous GPS sites, and this remains a topic of current investigation.

Most of the spatial and temporal variation in crustal deformation in Alaska can be described in terms of one or more of these four main processes:

- Postseismic deformation after the 1964 earthquake.
- Translation and rotation of large crustal blocks or plates.
- Spatial variations in plate coupling/slip deficit.
- A large SSE in Cook Inlet, 1998–2001.

These processes are described in further detail in the remainder of this section. *Fletcher* [2002] made a first attempt to construct combined models for the first three processes. Postseismic deformation after the 2002 Denali fault earthquake [*Freed et al.*, 2006a, 2006b] is not discussed in this paper, and the time range of the data presented here was chosen to avoid effects from the earthquake.

4.1. Postseismic Deformation

A decade ago, we were surprised to find that significant horizontal postseismic deformation from the 1964 earthquake continued into the 1990s. Work done in the 1970s had documented a large postseismic signal, but suggested a relatively short time decay constant of a few years [*Brown et al.*, 1977]. Tide gauge [*Savage and Plafker*, 1991] and VLBI [*Ma et al.*, 1990] data from Kodiak suggested that present uplift rates were higher than pre-earthquake rates, but for most of the 1964 rupture zone we expected to see no remnant of postseismic deformation. The first repeat surveys of GPS sites on the Kenai Peninsula, in 1995, showed that postseismic deformation still contributed 10–20 mm/yr to the present-day velocity field [*Cohen and Freymueller*, 1997]. Further measurements, resulting in the velocity field presented in section 3, showed that the postseismic signal extended along the entire length of the 1964 rupture, but not beyond, and it clearly affected sites as far away as the Alaska Range [*Zweck et al.*, 2002].

Early work on the 1964 postseismic deformation was based mainly on cumulative postseismic uplift data, determined by comparing 1990s GPS survey heights (corrected for geoid variations) with 1960s leveling heights [*Cohen et al.*, 1995; *Cohen and Freymueller*, 1997, 2004]. These data revealed large cumulative uplifts across the Kenai Peninsula (Figure 14). The cumulative 30-year uplift reached 90 cm in the middle of the Kenai Peninsula and more than 1 m at Turnagain Arm, and is offset from the region of peak coseismic subsidence. The 1990s viscoelastic relaxation models did not predict the observations, and in fact predicted subsidence where large uplift was observed. *Suito et al.* [2003] showed

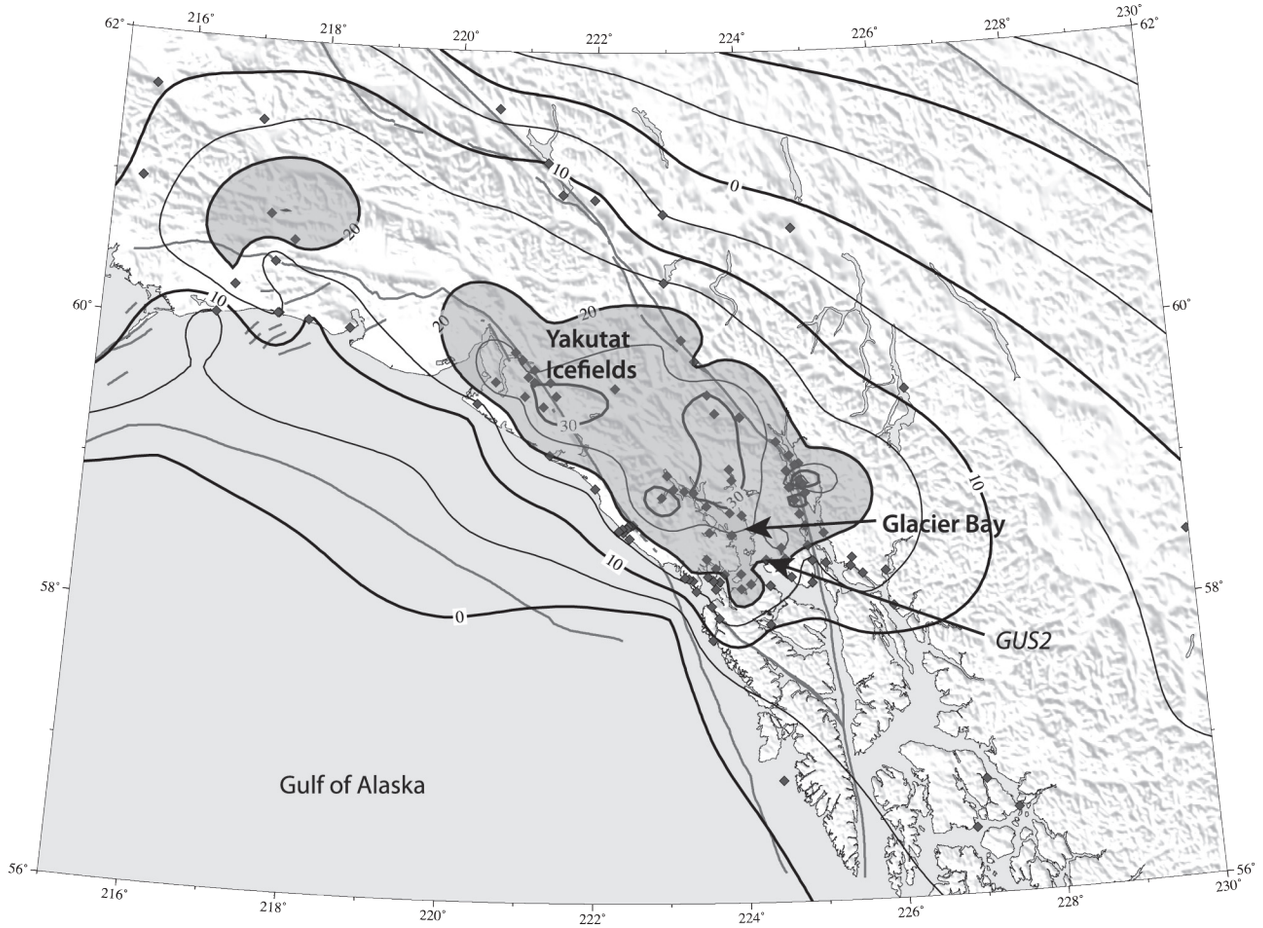

Figure 12. Contoured uplift rates in southeast Alaska, in mm/yr. The sites used in generating the contours are shown with diamonds. The shaded area outlines regions with uplift rates greater than 20 mm/yr. Site GUS2 (Figure 13) is labeled in italics.

that the earlier viscoelastic models had assumed the wrong model geometry, most importantly using a dip angle for the slab that was too steep. This error caused the region of postseismic subsidence in the viscoelastic models to be shifted toward the trench, relative to a model with the correct (shallower) dip. In addition, the 3-D effects from the presence of the dipping elastic slab caused a large change in the viscoelastic relaxation signal. Even when they did not predict the wrong sign of the deformation, all viscoelastic models predicted considerably less uplift than was observed. However, the cumulative uplift measurements can be explained easily by afterslip, which is continued postseismic slip on the fault plane or its downdip extension. This led *Cohen et al.* [1995] and *Cohen and Freymueller* [1997] to conclude that at least ~2.5 m of afterslip had occurred during the 30 years after the earthquake.

While the 30-year cumulative uplift data are explained mainly by afterslip, does the same hold true for the present-day velocities? Is the postseismic deformation still occurring today a continuation of afterslip 30 years later? Or is it related to other processes? *Zweck et al.* [2002] were able to fit an earlier version of the velocity field using an afterslip model (Plate 2a), but this model did not predict velocities in the area of the Alaska Range well. Also, the *Zweck et al.* [2002] model predicted afterslip continuing to depths of 70–100 km on the plate interface, probably too deep to reasonably expect afterslip. These and other results led us to develop an improved viscoelastic model for the earthquake (Suito and Freymueller, submitted manuscript, 2008), whose results are briefly summarized here.

The new viscoelastic model features an elastic slab that separates the sub-Pacific mantle and sub-Alaskan mantle

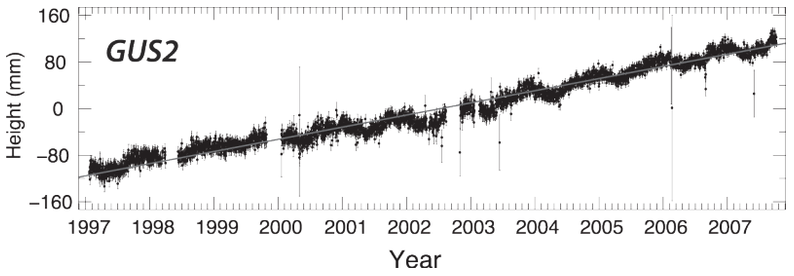

Figure 13. Vertical time series for GUS2 in Gustavus, showing the seasonal vertical signal at a representative continuous GPS site. A seasonal height variation of 17 mm peak to peak is superimposed on an uplift rate of 20.0 ± 0.15 mm/yr. The seasonal variation involves subsidence in winter and uplift beginning in April/May with the beginning of snow melt and runoff.

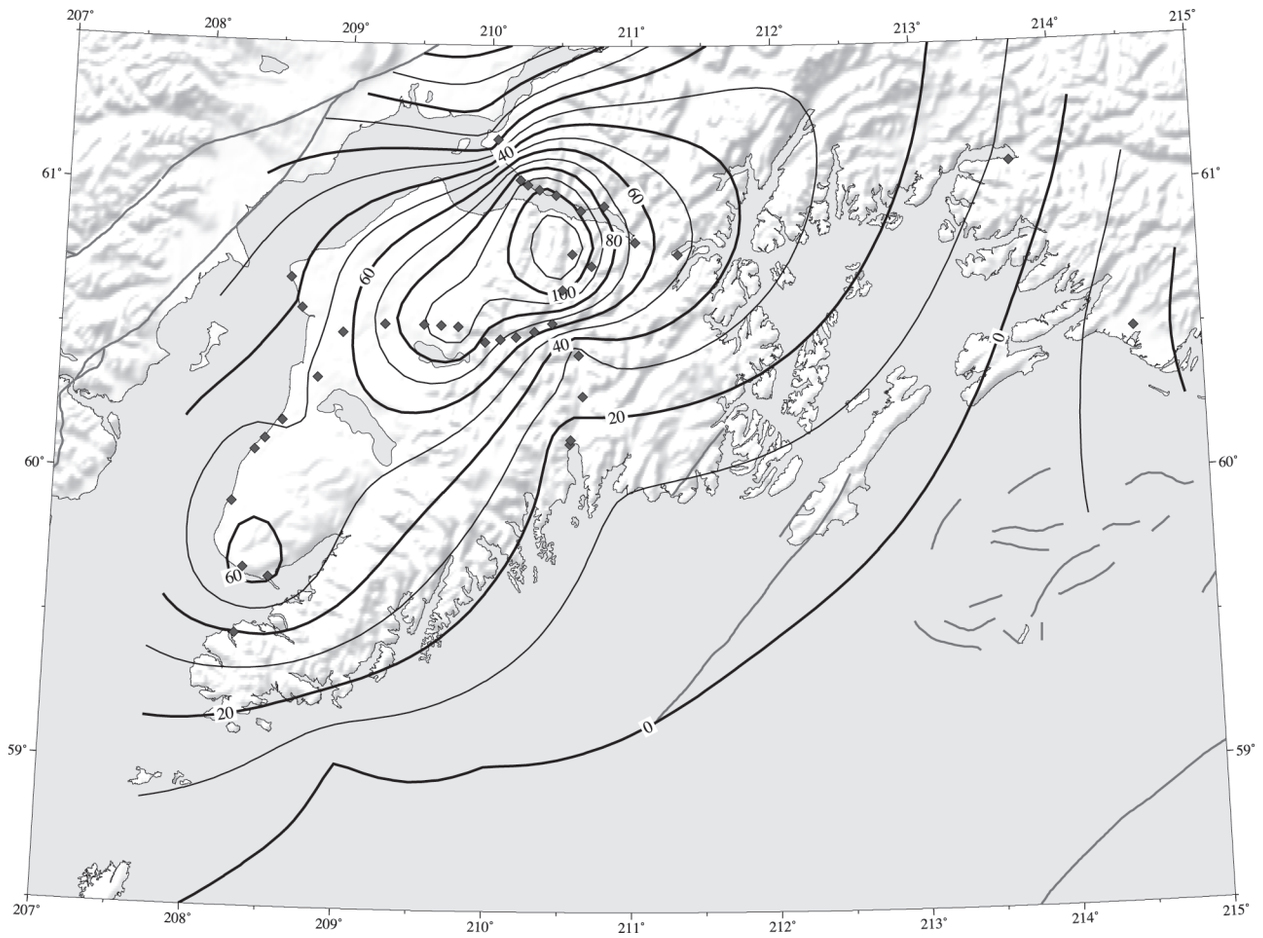

Figure 14. Contours of cumulative postseismic uplift (shown with black lines), Kenai Peninsula, in cm. Uplift data are based on leveling measurements from 1964 to 1965, compared to GPS heights from 1995 to 2000, with correction for the geoid–ellipsoid offset. Lines denote Quaternary and Holocene faults from *Plafker et al.* [1994].

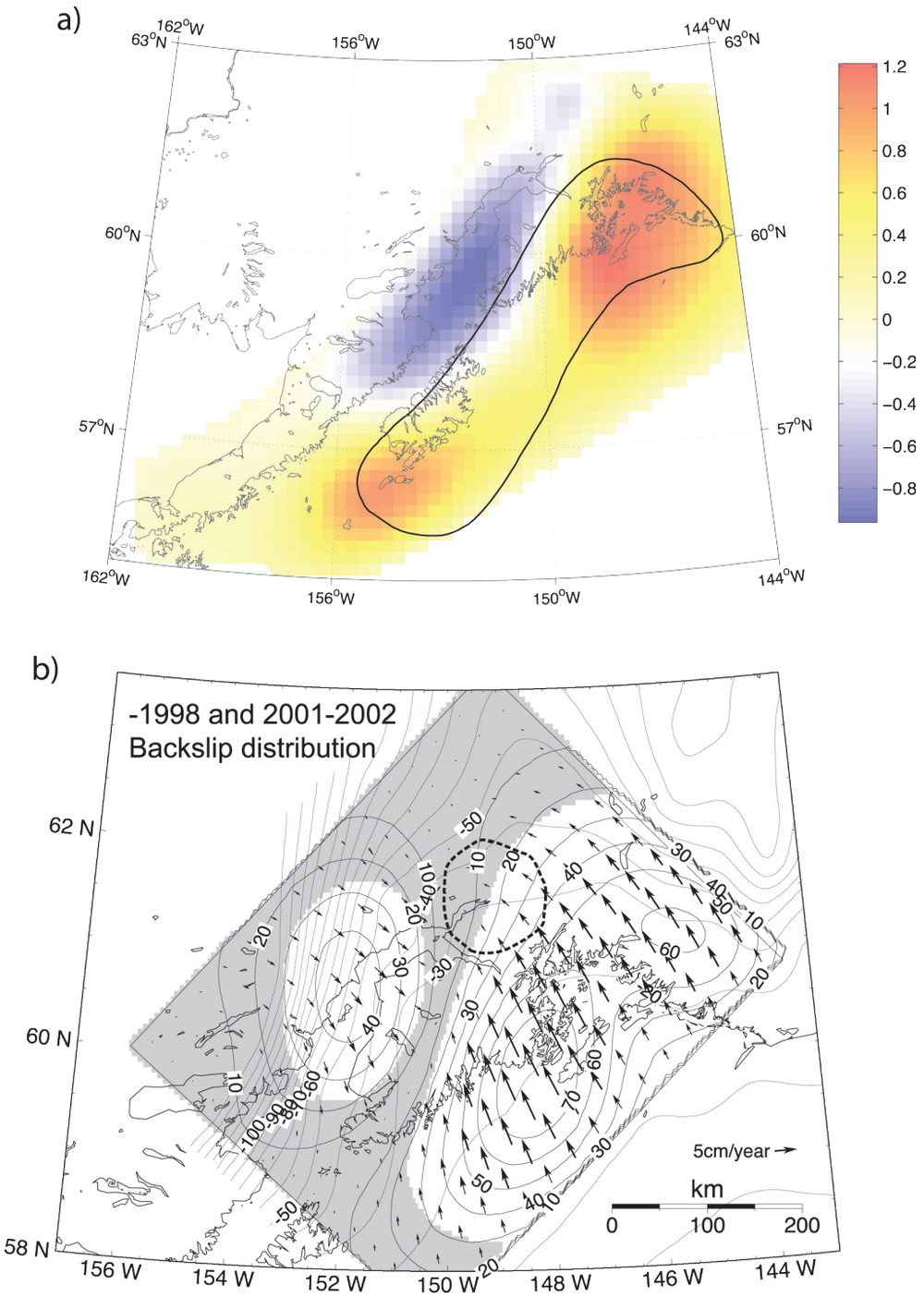

Plate 2. (a) The *Zweck et al*. [2002] coupling model. Hot colors indicate the region of high slip deficit, and blue colors indicate regions of afterslip. (b) *Ohta et al.* [2006] coupling model for the periods with no slow-slip events. The area of the 1992–2001 slow-slip event is shown by a heavy dashed line in Plate 2b. The velocities used by *Ohta et al.* [2006] were corrected for postseismic deformation from the 1964 Alaska earthquake using the viscoelastic model of Suito et al. (submitted), whereas the *Zweck et al*. [2002] velocities were not. Correction for the viscoelastic deformation largely eliminated the region of estimated afterslip, and extends the estimated region of slip deficit farther downdip.

into two separate regions of flow, with the slab geometry based on seismic constraints summarized by *Zweck et al.* [2002]. Both regions of the mantle were assigned the same (Newtonian) viscosity, which we varied over a range of values, resulting in relaxation timescales τ ranging from 1 to 35 years. The relaxation is not complete during the first 40 years, so all viscoelastic models predict significant displacements today, and the predicted present velocities increase in magnitude as the relaxation time is reduced (assuming $\tau \geq 5$ years). The model predicts key features of the present horizontal velocities well, as long as the relaxation timescale τ is 25–35 years. For example, with $\tau = 5$ years, the model predicts present horizontal trenchward velocities of ~30 mm/yr on the Kenai Peninsula (1.5–2 times that observed), ~20 mm/yr at the Alaska Range, and >10 mm/yr in the Fairbanks area (several times that observed), but for $\tau = 25$–35 years the predictions are a good match for the observations in these areas. The model predicts trenchward motion for sites as far away as Fairbanks, 2–3 mm/yr at that distance (Figure 15), with sites near the Alaska Range moving about twice as fast. The trenchward velocities in the western Kenai/Cook Inlet region are slightly smaller than the observed rates, or about 15 mm/yr peak velocity.

The region of trenchward motion is largely confined to the rupture zone, and expands laterally only slowly with distance from the trench. *Ohta et al.* [2006] showed that when the velocities in the Kenai Peninsula to Cook Inlet region are corrected for viscoelastic relaxation, the area of afterslip estimated by *Zweck et al.* [2002] almost completely disappears, and the region of estimated plate coupling extends significantly farther downdip (Plate 2b). This improved coupling model also makes the interpretation of the position of the 1998–2001 SSE more easily understood (see section 4.4). Thus, even 30 to 35 years after the earthquake, the present-day velocities contain a significant component of postseismic viscoelastic relaxation, which produces trenchward motion and uplift. Most, if not all, of the trenchward motion in the Cook Inlet region, first observed by *Cohen and Freymueller* [1997] and modeled in terms of afterslip by *Freymueller et al.* [2000] and *Zweck et al.* [2002], can be explained as resulting from viscoelastic relaxation.

For all plausible relaxation times, the predicted cumulative uplift from viscoelastic relaxation is small compared to the observed uplift. Predicted uplift from viscoelastic relaxation is 20–40% of the observed cumulative uplift at the western side of Kodiak Island (Figure 1a), and less than 10% at the eastern side of the island. Around the Prince William Sound asperity, the largest predicted uplifts are along the southeastern coast of Cook Inlet and the western Kenai Peninsula (Figure 1a), but the predicted uplifts are never more than 50% of the observed uplifts, and only 10–20%

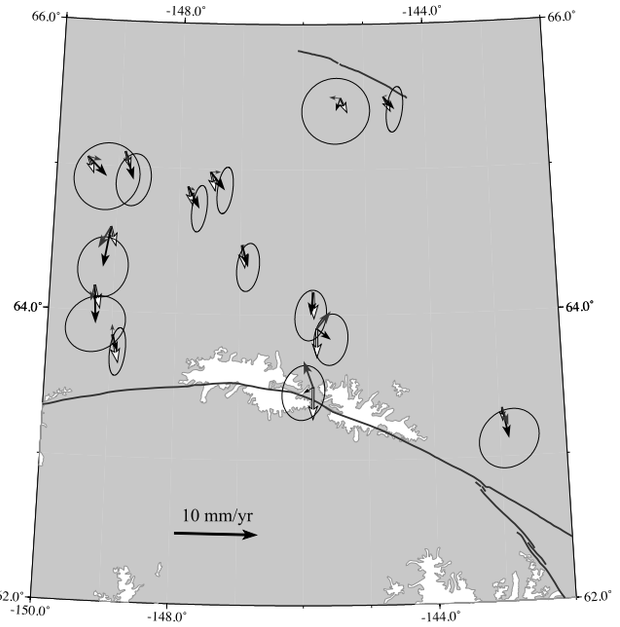

Figure 15. Velocities of sites north of the Alaska Range, compared to postseismic model predictions. Observed velocity vectors are in black, with 95% confidence ellipses, and the velocities predicted by the viscoelastic model of Suito and Freymueller (submitted manuscript, 2008) are shown in white. Residual vectors are shown in gray. Active faults are shown in black, and white areas are high glaciated topography.

over most of the region. The reason for this follows from the geometry of the problem. Given the thickness of the overriding continental crust and the shallow dip angle of the slab, the slab remains in contact with the overriding crust even to the north of Cook Inlet [*Abers et al.*, 2006; *Ferris et al.*, 2003; *Veenstra et al.*, 2006]. The presence of the elastic slab restricts the region of viscoelastic relaxation to the mantle wedge, and this severely limits the potential for viscous flow to generate uplift. Models that neglect the effect of the slab predict larger uplift, but even in these cases the deformation caused by viscous flow is mainly horizontal.

The results of the viscoelastic model highlight an intriguing feature of the available postseismic data sets for the 1964 Alaska earthquake. We have data covering two very different periods, the 30-year cumulative uplift and the present-day velocities, and each of these data types is sensitive mainly to one mechanism of postseismic deformation. The cumulative 30-year uplift data are sensitive mainly to afterslip, whereas the far-field postseismic deformation in the present velocities is dominated by viscoelastic relaxation. This feature of the data sets makes it possible to constrain the mechanisms separately and then determine a combined, multimechanism

model (Suito and Freymueller, submitted manuscript, 2008). In particular, the continuous tide gauge record at Kodiak Island along with cumulative uplifts determined from repeat measurements of tidal bench marks in the Kodiak archipelago [*Gilpin*, 1995; *Gilpin et al.*, 1994] can be explained by a combination of viscoelastic relaxation and ~6 m of afterslip (Suito and Freymueller, submitted manuscript, 2008).

Comparison of the plate coupling models of *Zweck et al.* [2002] and *Ohta et al.* [2006] shows that the earlier paper underestimated the downdip width of the region of high slip deficit (Plate 2), although the along-strike variations found by *Zweck et al.* [2002] are robust features and are not affected by the neglect of viscoelastic relaxation.

4.2. Spatial Variations in Subduction Zone Coupling, Segmentation, and Persistence of Asperities

4.2.1. Subduction seismic cycle models. Most models for interseismic deformation at subduction zones are based on the method of *Savage* [1983]. In that model, the slip distribution on the plate interface is represented by a superposition of steady slip at the plate convergence rate with backward slip on the shallow seismogenic region, to cancel the forward slip on the part of the interface that does not move between earthquakes. We follow the usual approach and extend the model of *Savage* [1983] by allowing the main thrust zone to be partially creeping, instead of requiring it to be fully locked. We define the slip deficit (rate) as the plate convergence rate minus the actual slip rate on the plate interface. There is no slip deficit if the slip on the interface occurs at the plate convergence rate, whereas if the plate interface is completely locked (no slip), then the slip deficit would be equal to the convergence rate. The slip deficit can be parameterized using a coupling coefficient, which is the slip deficit divided by the plate convergence rate. The spatial resolution of subduction zone slip deficit models varies tremendously, depending on the distribution of data, but even in the best areas the real model resolution is often no better than 30–50 km. The position of the downdip end of the locked zone is always resolved much better than the position of the updip end, which is often almost completely unconstrained unless there are sites very close to the trench. Along parts of the southern Alaska subduction zone, such as the Shumagin segment (Figure 1a), there are islands located in the forearc region, which allow better resolution of the updip extent of the locked zone compared to most subduction zones worldwide.

The Savage model is a kinematic model that by itself does not tell us about the mechanical properties or stress state of the plate interface. Within the main seismogenic zone, friction is the dominant force that resists fault creep, but if friction is spatially variable then the rate of creep of the interface will depend on both the distribution of frictional properties and the elastic properties of the lithosphere. When we refer to "locked zones," we refer to regions of high slip deficit, which are kinematically locked. In general, we will make the assumption that these locked zones are stationary in time, to first order, although the downdip width of the locked zone does vary somewhat in time wherever there are SSEs.

Postseismic deformation also impacts the slip deficit distribution on the plate interface. After a major earthquake, afterslip downdip of, and possibly within, the coseismic rupture zone is commonly observed, as it was for the 1964 earthquake. Regions undergoing afterslip may slip much faster than the average rate of plate motion, producing a negative slip deficit for a certain period. Thus, a kinematic snapshot taken shortly after an earthquake will not reflect the long-term slip deficit distribution, but afterslip appears to decay away over a small fraction of the earthquake recurrence time, and later the slip deficit distribution may reflect the long-term average between earthquakes. Viscoelastic relaxation in the asthenosphere and/or crust can also produce significant deformation, and if this is not modeled it can bias the slip deficit distribution estimated using the Savage model. However, when corrections to the observations are made based on a realistic model of viscoelastic relaxation, the slip deficit distribution from the Savage model agrees well with the extent of the seismogenic zone of the plate interface inferred from great earthquake ruptures [*Cross and Freymueller*, 2007, 2008; *Ohta et al.*, 2006].

GPS velocities of sites near a subduction zone may be composed of two components: the interseismic strain caused by the slip deficit of the main thrust zone, and a rigid body motion due to motion of the arc itself. This rigid body motion must be modeled together with the interseismic strain. In most cases, the reference frame for the velocities is taken to be the stable interior of the overriding plate, so the rigid body motion would represent the motion of the forearc block relative to the overriding plate. Both slip partitioning of oblique subduction and rotations of forearc blocks are common features at subduction zones [e.g., *McCaffrey*, 1992; *McCaffrey et al.*, 2000; *Wallace et al.*, 2004, 2005], and forearc motions can have a major impact on the deformation model. In some cases, ignoring motion of the forearc will cause only a small coherent residual, but in other cases the block rotation has a major impact on the estimates of slip deficit. See *McCaffrey* [2002] for a detailed discussion. Where block rotations are rapid, the block rotation can dramatically impact the convergence rate at the subduction zone [*Wallace et al.*, 2005], although this is a minor effect in Alaska. The major rotating blocks of the overriding plate will be discussed in section 6.

4.2.2. Along-strike subduction zone variations in Alaska. The Alaska subduction zone displays strong along-strike variations in the behavior of the shallow seismogenic zone. Both the width of the zone locked between earthquakes and the magnitude of the slip deficit vary dramatically, often over along-strike distances that are short compared to the width of the locked region [*Cross and Freymueller*, 2007, 2008; *Fournier and Freymueller*, 2007; *Ohta et al.*, 2006; *Zweck et al.*, 2002]. Models for the slip deficit distributions for segments comprising most of the Alaska–Aleutian arc are found in the previously cited papers, and results of these models are summarized in Plate 3. Dark shaded regions in the figure indicate areas of significant slip deficit (locked regions), whereas yellow shaded regions are dominantly or entirely creeping, and other regions have too little data to tell.

The overall picture is that variation in the seismogenic zone is the rule rather than the exception, and any effort to characterize the seismogenic zone in terms of simple variables that vary slowly along strike (e.g., the temperature distribution, plate velocity, or the amount of sediment in the trench) is doomed to failure. Similar variations are seen at other subduction zones, such as northern Japan [*Suwa et al.*, 2006] and Hikurangi (North Island, New Zealand) [*McCaffrey et al.*, 2008; *Wallace et al.*, 2004]. The locations and extents of the locked regions also correspond to first order to major features of the 20th century earthquake history, which will be discussed further in the next section.

The 1964 earthquake rupture zone was about 800 km long and features two large segments with a very wide locked region, 200–250 km wide in the downdip direction, separated by an intervening segment that is dominated by creep [*Ohta et al.*, 2006; *Zweck et al.*, 2002]. This matches the distribution of slip in the 1964 earthquake, which had a region of low slip between areas of high slip in Prince William Sound and Kodiak Island [*Holdahl and Sauber*, 1994; *Ichinose et al.*, 2007; *Johnson et al.*, 1996; Suito and Freymueller, submitted manuscript, 2008]. The eastern locked region might be broken into two separate regions, based on the presence of two distinct regions of subsidence separated by a linear zone of essentially zero vertical motion that lies at the extreme western edge of Prince William Sound. One region of subsidence corresponds to eastern Prince William Sound, and the other is located offshore of the Kenai Peninsula. *Brocher et al.* [1994] and *von Huene et al.* [1999] suggested that the 1964 rupture in Prince William Sound might have ruptured parts of both the Yakutat–North America and Pacific–North America plate interfaces, and the narrowing of the subsidence bowl west of Montague Island corresponds to the subsurface edge of the Yakutat terrane. There is a significant gap between the Prince William Sound and Kodiak asperities that is dominated by creep (Plate 2). The transition from the wide locked zone to the narrow locked zone causes the dramatic contrast in present-day velocities noted by *Freymueller et al.* [2000] and shown in Figure 4. The along-strike width of the transition is a matter of continuing research, but must be much smaller than the 200-km width of the locked zone under Prince William Sound.

The detailed shape of the locked region under Kodiak Island is uncertain, mainly due to a lack of data from the central part of Kodiak Island. *Savage et al.* [1999] analyzed data from a profile at the SW end of Kodiak Island, whereas *Sauber et al.* [2006] also analyzed data from a profile at the NE end of the island. *Savage et al.* [1999] found a very wide locked zone (~150 km) at the SW end of Kodiak Island. *Sauber et al.* [2006] presented the locked zone in terms of its depth extent rather than its width, but confirmed that the seismogenic zone is wide across all of Kodiak Island. *Zweck et al.* [2002] used the data of *Savage et al.* [1999], but not those of *Sauber et al.* [2006], and thus had limited resolution for NE Kodiak (Plate 2a). The wide zone of slip deficit at Kodiak continues to the SW along the length of the 1938 rupture zone (Figure 1a), then narrows and has a shallower downdip limit in the Shumagin segment (also featuring more creep), and ends abruptly at the western edge of the Shumagin Islands [*Fletcher et al.*, 2001; *Fournier and Freymueller*, 2007; *Freymueller and Beavan*, 1999]. *Zweck et al.* [2002] could not resolve any low slip deficit "gap" between the Kodiak segment of the 1964 rupture zone and the 1938 rupture zone, but given the data distribution a gap of a few 10s of km length would not be resolvable.

There is a long segment dominated by creep extending from the Shumagin Islands west to the Fox Islands. The abundant data from the Sanak segment at the western end of the Alaska Peninsula require that the plate interface be creeping almost out to the trench; *Freymueller and Beavan* [1999] estimated that the maximum allowable width of a locked zone was 35 km, and only if its updip limit was exactly at the trench. Using an updated data set with more precise velocities, *Fournier and Freymueller* [2007] showed that the downdip limit of any locked zone could be no deeper than 11 km, which makes it likely that there is no locked zone at all in this segment. Data from the rest of this creeping segment come mainly from volcano networks, and small variations in the tectonic signal may be difficult to differentiate from volcanic deformation signals. However, there is no evidence of a significant locked region on the plate interface until the western end of Umnak Island [*Cross and Freymueller*, 2008]. There is a region of no data about 150 km long west of Unimak Island, and perhaps this is large enough to contain a locked region corresponding to the 1946 Scotch Cap earthquake rupture zone, although this would locate that earthquake farther west than the most recent seismological estimates [*López and Okal*, 2006].

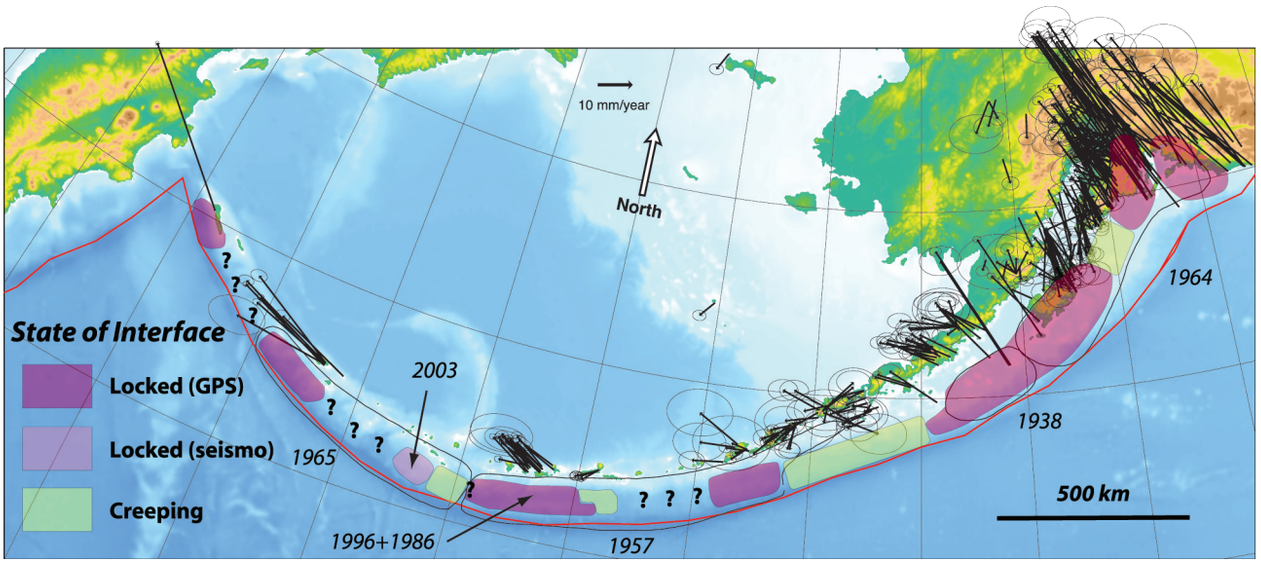

Plate 3. Plate coupling variations along the arc. Colored regions indicated the state of the plate interface, with dark areas indicating locked regions (significant slip deficit). Darker shading indicates that the locked region is based on GPS data, whereas lighter shading indicates an assessment based on seismic ruptures alone. Regions shaded in yellow are inferred to creep, whereas areas shown with question marks do not have enough data to determine the state of the plate interface.

Cross and Freymueller [2007, 2008] showed that the Andreanof Islands also featured strong along-strike variations in the seismogenic zone. They found a wide region of high slip deficit corresponding to the combined rupture zones of the 1986 M_w = 7.9 Andreanof Islands earthquake and the 1996 M_w = 7.9 Delarof Islands earthquake to the west of it. The earthquake rupture zones are shown in Figure 1a. In contrast, east of the 1986 rupture zone they found a region of low slip deficit, dominated by creep, which extends at least as far as the island of Atka. The region of high slip deficit represents the eastern one-third of the 1957 M_w = 8.9 earthquake rupture zone (Figure 1a), which had high slip in the earthquake, whereas the remainder of the 1957 rupture zone had relatively low slip [*Johnson et al.*, 1994]. It is particularly intriguing that the tsunami-based model of *Johnson et al.* [1994] for the 1957 earthquake featured only one other area of high slip east of the Andreanof islands, at western Umnak Island. That corresponds to the only region of high slip deficit that we can identify between the Andreanof Islands and the Shumagins.

Parts of the central and western Aleutians lack geodetic data, and we have no information about the state of the plate interface there. However, the occurrence of the 2003 M_w = 7.8 Rat Islands earthquake (Figure 1a), and its similarity to the first part of the 1965 M_w = 8.7 Rat Islands earthquake (S. Beck, personal communication, 2006), suggest that the seismogenic zone in the western Aleutians is composed of alternating locked and creeping regions as well. The 1965 M_w = 8.7 Rat Islands earthquake ruptured three distinct asperities, of which the 2003 event appears to have reruptured the easternmost. The locked region we see with GPS in the area of Attu Island corresponds to the second asperity of the 1965 rupture. There is no GPS data from the area of the westernmost asperity. These observations are consistent with the hypothesis that the 1965 earthquake ruptured three distinct asperities with small creeping zones between them, which allowed the asperities to rupture independently. Implicit in this hypothesis is the idea that an asperity either ruptures completely or not at all in a given earthquake, which remains to be verified, and the creeping zones between the asperities are inferred by comparison to the 1964 earthquake rupture zone.

Lu and Wyss [1996] evaluated the stress segmentation of the Aleutian arc using earthquake focal mechanisms. They identified five segments, each with constant stress tensor orientation, and discussed the relationship between the stress segment boundaries and both fracture zones on the downgoing plate and earthquake rupture zones. In general, σ_1 is oriented between the direction of motion of the Pacific plate and the trench-normal direction, which is consistent with the stress being dominated by plate convergence, and by the development of slip partitioning in the western Aleutians. In general, either σ_2 or σ_3 is vertical, and the other is oriented in a roughly trench-parallel direction. However, the plunge of σ_1 varies from segment to segment, and the orientations of σ_2 and σ_3 swap between horizontal and vertical. Two of the four boundaries between their stress segments fall in regions we identify as being dominated by creep, and the edge of the final segment falls between the two main rupture areas of the 1964 earthquake. One segment boundary falls between the 1986 and 1996 earthquake rupture zones in the Andreanof Islands, and this segment (segment III of *Lu and Wyss* [1996]) probably reflects a region of reduced shear stress after the 1986 earthquake. Compared to the segment west of it, after the 1986 earthquake σ_1 is rotated toward a more vertical direction, and the vertical stress has been reduced so that σ_2 is now horizontal rather than vertical. We hypothesize that after the 1996 Delarof Islands earthquake, the stress tensor there would be similar to that of the 1986 rupture zone identified by *Lu and Wyss* [1996]. Note that this earthquake occurred after the report of *Lu and Wyss* [1996] came out, so this hypothesis can be tested, with future work.

Overall, however, there is no clear relation between the stress segments identified by *Lu and Wyss* [1996] and the locked and creeping zones we identified with geodesy. A study of stress variations using segment boundaries defined by the locked and creeping regions identified geodetically might prove enlightening. However, the fact that *Lu and Wyss* [1996] identified the 1986 earthquake rupture zone as a distinctive stress segment might mean that the earthquake stress drop is a significant fraction of the total stress in the shallow crust in subduction zones. If this is true, stress segmentation may be strongly time-dependent.

4.2.3. The asperity model and persistence of asperities. The segmentation of great earthquakes at subduction margins has long been a critical problem. Why great earthquakes rupture the areas they do, whether those rupture areas are repeatable, and how often they recur are critical questions that must be answered before we can understand the physics that controls great earthquake ruptures and the seismic hazards associated with subduction zones. Based on purely seismological observations, *Thatcher* [1990] summarized two end-member models, the asperity model and the uniform coupling model, which have been used to describe plate coupling and the recurrence of great earthquakes at convergent plate margins. Geodetic observations from Alaska support *Thatcher*'s [1990] conclusion that the asperity model better explains the observations, and suggest that asperities are persistent features of the shallow plate interface.

In the asperity model, the plate interface is divided into a patchwork of high stress (asperities) and low stress regions.

High stress regions are those that require a large shear stress to fail, whereas the low stress regions fail at much lower shear stresses. In terms of the rate and state friction formulation, the asperities are considered to represent frictionally unstable regions (velocity weakening), surrounded by frictionally stable regions (velocity strengthening) [e.g., *Bilek et al*., 2004]. Low stress regions could also be regions that exhibit stick-slip behavior but fail at a relatively low shear stress, because of asperity size or some other form of weakness. Unless the frictional properties of the interface evolve rapidly in time, the asperities should be persistent features and successive great earthquakes will rupture one or more adjacent asperities. Although successive great earthquakes may differ in that each may rupture a different set of asperities, the slip distributions of successive ruptures in a given section of the margin will reflect the shape and distribution of the asperities.

The persistence of asperities can be tested by comparing slip distributions of past great earthquakes to the slip deficit distributions inferred from geodetic measurements. As noted in the previous section, there is a good first-order correlation between the regions of high slip deficit identified by our geodetic data (Plate 2) and the asperities of the last set of great earthquakes. Equally important, we find regions of low slip deficit in the areas that had low slip in the last set of great earthquakes. This is most obvious in the case of the 1964 earthquake, where a region of low slip separated the large Prince William Sound and Kodiak asperities, and the same pattern appears in the distribution of slip deficit [*Zweck et al.*, 2002]. Two key assumptions are made in making this comparison. First, we assume that the slip deficit distribution is stationary in time, making the present-day distribution a reasonable proxy for the entire interseismic period. Second, we assume that all interseismic slip deficit is released coseismically, instead of through postseismic slip or some other mechanism. These assumptions are more likely to be correct when considering along-strike variations, as we do here, than for downdip variations.

West of the 1964 rupture, a strong test of the correlation between seismic asperities and regions of high slip deficit can be made only for parts of the earthquake rupture zones, due to a lack of data on either the geodetic or seismic side. However, a good correlation is found for the 1938 earthquake rupture zone (Alaska Peninsula), the western half of the 1957 rupture zone (Andreanof Islands), and the western end of the 1965 rupture zone (Near Islands). In the case of the 1957 earthquake, most of the slip occurred in the western third of the rupture, in the area that reruptured in the 1986 and 1996 earthquakes, and low slip occurred immediately to the east of the 1986 rupture zone. This matches the pattern of slip deficit inferred from geodesy. *Johnson et al.* [1994] identified only one region of high slip in the eastern half of the earthquake rupture, located 50 km west of Okmok Volcano (Figure 10). Although geodetic data are sparse in that part of the rupture zone, that same area is also the only place in the Fox Islands that shows a significant region of high slip deficit [*Cross and Freymueller*, 2008].

The correlation of present zones of slip deficit with past zones of high slip in earthquakes is strong evidence that the seismic asperities are persistent from earthquake to earthquake. Complementary evidence comes from the correlation of features in the forearc, which require a long time to develop, with seismic asperities. *Wells et al.* [2003] and *Song and Simons* [2003] independently identified a correlation between regions of high slip in earthquakes and relative gravity lows. *Song and Simons* [2003] showed that this correlation was global in nature, with about 75% of the seismic moment coming from the 25% of the forearc areas with lowest gravity, relative to the average for that trench. *Wells et al.* [2003] highlighted the relationship between forearc basins, gravity lows, and the zones of high slip in earthquakes; they proposed that subduction erosion may be higher in the regions of seismic slip, causing the long-term development of forearc basins centered over the regions of seismic slip. Regardless of the exact mechanism involved, both papers support the idea that asperities are persistent over geologic timescales.

Our estimate of the location of asperities along the Alaska–Aleutian trench has strong similarities to that of *Wells et al.* [2003], but with some significant differences. In the 1957 rupture zone, *Wells et al.* [2003] suggested that high slip occurred beneath the Atka Basin in both 1957 and 1986, whereas we find most, if not all, of the Atka Basin to be underlain by a region of low slip deficit (Figure 10). The limits of 1957 slip are quite uncertain due to limited data, but the distributed slip (seismic) models for the 1986 event seem to show little to no slip beneath the Atka Basin in that event [*Boyd and Nabelek*, 1988; *Ekström and Engdahl*, 1989; *Houston and Engdahl*, 1989], which agrees more with our result. In this case, the seismic asperity seems to correlate more clearly with the Hawley Ridge and its paired forearc basin, rather than the deeper Atka Basin. However, for the rest of the 1986 and 1996 earthquake rupture zones, our estimate of the asperity location agrees with that of *Wells et al.* [2003]. In the 1964 rupture zone, *Wells et al.* [2003] noted that slip in the earthquake showed an ambiguous relationship with forearc gravity lows. The region of high slip in Prince William Sound follows a relative gravity low, but farther to the SW the region of high slip follows a relative gravity high instead. This may be due to the anomalous, outer-arc gravity high related to the subduction and accretion of the Prince William and Yakutat terranes beneath North America. The

relationship between gravity lows and the asperities in the 1938 rupture zone (Figure 8) is also less clear. The large Tugidak forearc basin SW of Kodiak Island correlates with a region of high slip deficit [*Fournier and Freymueller*, 2007], but we find the wide region of slip deficit to be continuous to the southwest across the Semidi Islands gravity high and the Shumagin forearc basin. However, this difference may be the result of data resolution limitations. We find the Shumagin Islands themselves, which are located on a gravity high, to be underlain by a smaller asperity or a region of weaker (but still nonzero) slip deficit.

4.3. Slow-Slip Event

In addition to the spatial variation in deformation discussed so far in this paper, we have observed temporal complexity as well, due to a large SSE that occurred in the upper Cook Inlet area. SSEs are a more general name for the slip events termed *episodic tremor and slip* events in Cascadia [*Rogers and Dragert*, 2003]. Cascadia SSEs thus far have always been paired with seismic tremor, but it is not clear whether that holds true everywhere [*Schwartz and Rokosky*, 2007]. Sites in the area north of Anchorage show coherent deviations from linear motion during the period 1998–2001 (Figure 16), whereas sites in the central Kenai Peninsula or far north of Anchorage show no deviation from a linear trend. Sites in this area generally moved northward with time prior to 1998, then moved rapidly southward from 1998 to 2001, and moved northward again afterward, until the time series were interrupted by the 2002 Denali Fault earthquake and its postseismic effects. The east components of motion (not shown) change almost linearly with time.

Ohta et al. [2006] divided the GPS time series into three periods—(1) before 1998, (2) 1998–2001, and (3) 2001–2002—where the second period contains the SSE. Site velocities during periods 1 and 3 were equal within uncertainties, and elastic slip deficit models estimated for both periods were identical in the areas where model resolution was good, so these periods were taken to reflect the steady deformation. The slip deficit distribution for these periods, corrected for 1964 viscoelastic postseismic deformation, is shown in Plate 2b, and the region of slow slip in 1998–2001 is highlighted in that figure. Comparing the SSE period to the time before and after, there were no changes to the slip deficit distribution in the shallow part of the seismogenic zone that corresponds to the main 1964 rupture area.

The downdip extent of the region of slip deficit estimated during the SSE period compares very well with the 1964 main slip zone, and the main slip zone appears to be kinematically locked during the entire study period. *Ohta et al.* [2006] proposed that the region of the SSE is part of a transition from a fully locked to a fully creeping portion of the interface, and that it fails repeatedly in SSEs, so that at the time of a large earthquake the shear stress on this part of the interface is very low in comparison to the main asperity updip of it. In this view, the SSE erased 5–15 years of slip deficit in the transition zone between the fully locked and fully creeping sections of the plate interface. A second and smaller SSE in 2005–2006 occurred in approximately the same location as the 1998–2001 event [*Ohta et al.*, 2007]. This shorter event lasted ~6 weeks, and slip in the event was much smaller than in the large event. It is possible that there have been additional small events in this same location, but there were not enough continuous GPS sites to rule out temporally correlated noise as an explanation for variations in the time series of sites ATWC and ATW2.

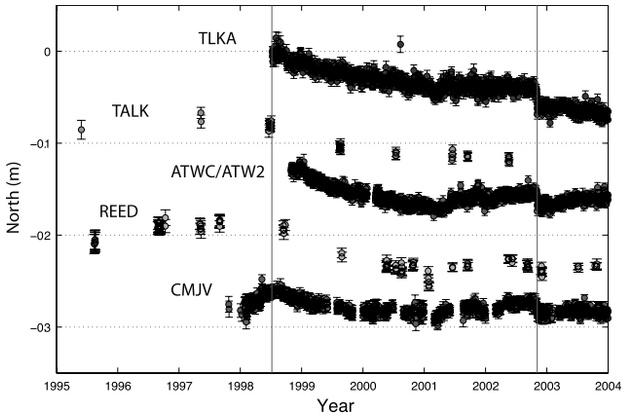

Figure 16. Time series for several sites in the region on the 1998–2000 slow-slip event in Cook Inlet. Sites are shown from north to south, Talkeetna (TLKA and TALK), Palmer (ATWC/ATW2 and REED), and Anchorage (CMJV). The time of the start of the slow-slip event (1998.5, based on CMJV) and the time of the 2002 Denali Fault Earthquake are shown by vertical lines.

There is no unequivocal evidence for other large SSEs in Alaska during the period 1995–2007, although there are a few anomalies that might be SSEs, but might also be noise. The earliest GPS surveys from lower Cook Inlet, mainly from the Kenai Peninsula and Augustine volcano, suggest the possibility of a large transient event ending in 1996, but we have not been able to rule out the possibility that this represents a systematic error. The CGPS site KDK1 in Kodiak shows what may be a transient event in early 1999. The site KODK in Kodiak shows an apparent offset in January 2003, but this was mainly in the east component (and KDK1 shows no offset).

Continuous GPS time series from the sections of the plate interface dominated by creep are mostly too short to be definitive, but the few long-term continuous GPS sites in areas of low slip deficit show linear motion over several years.

Sites in Cold Bay (BAY1, 11 years) and Seldovia (SELD, 7 years) do not show significant deviations from their linear trends. This observation leads us to suggest that these creeping interfaces do not creep episodically in large SSEs, but instead creep on a steady basis. This is different from the case of the Japanese Ryukyu Islands, where the long-term strain from subduction is small because of biannually repeating SSEs that involve most or all of the potentially seismogenic interface [*Kataoka and Heki*, 2007; K. Heki and T. Kataoka, On the biannually repeating slow slip events at the Ryukyu Trench, southwestern Japan, submitted to *J. Geophys. Res.*, 2008]. However, some of the segments we infer to creep have only campaign GPS data, and we cannot rule out a Ryukyu-like behavior for parts of the plate interface in Alaska.

4.4. Subduction Geometry Beneath Prince William Sound

The motion of the Yakutat terrane, and the possibility that it extends in the subsurface as subducted material far to the NW of its subaerial extent [*Ferris et al.*, 2003; *Fuis et al.*, 2008], supports the hypothesis that there are two active subduction interfaces beneath Prince William Sound [*Brocher et al.*, 1994; *von Huene et al.*, 1999]. In this conception, the Yakutat terrane subducts toward ~N35°W beneath the overriding plate (geologically, the Prince William terrane), whereas the Pacific plate subducts beneath the combined North American plate and Yakutat terrane. This could result in two seismogenic interfaces beneath Prince William Sound, a shallower Yakutat–North America interface, and a deeper Pacific–Yakutat interface. To the southwest, where the Yakutat terrane pinches out near the edge of Montague Island (Figure 4), these two interfaces would merge into a single subduction interface between Pacific and North America. This geometry would result in two distinct directions for slip on the interfaces, roughly N35°W for Yakutat–North America and N12°W for Pacific–North America. Pacific–Yakutat relative motion is <20 mm/yr and is directed to the NE [*Fletcher and Freymueller*, 1999, 2003].

The geodetic data support this hypothesis. Present-day velocities rotate from roughly the Yakutat–North America direction at the eastern edge of Prince William Sound to the Pacific–North America direction at the western edge. There is a corresponding rotation in the coseismic displacements from the 1964 earthquake [*Parkin*, 1972]. The pattern of vertical velocities may also support this hypothesis, although not as clearly.

There is a discrepancy between the recurrence interval of great earthquakes in Prince William Sound and the Pacific–North America plate convergence rate, which would be reduced or eliminated if the 1964 coseismic slip beneath Prince William Sound was on the Yakutat–North America interface instead. *Carver and Plafker* [this volume] estimated the recurrence interval for great earthquakes in Prince William Sound to be 589 years (median intervals vary from 333 to 875 years, depending on site), based on the paleoseismic record. However, at a convergence rate of 55 mm/yr appropriate for Pacific–North America relative motion, ~20–25 m of slip deficit would accumulate in ~360–450 years, significantly less than the average interval between earthquakes. Yet, all geodetic data after the earthquake supports the idea that the plate interface beneath Prince William Sound is completely locked and does not slip between earthquakes. This mismatch could be explained if the typical coseismic slip beneath Prince William Sound is larger than that of the 1964 earthquake, or if the total slip in smaller earthquakes is a significant fraction of that in great earthquakes, or if the shortest median intervals are the most representative in the paleoseismic record, or if very large creep events occur within the seismogenic region. Although these cannot be ruled out entirely, all are unlikely. However, if the slip rate beneath Prince William Sound is assumed to represent the Yakutat–North America motion, then 20–25 m of slip corresponds to a recurrence interval of 500–625 years, in excellent agreement with the average geologically observed recurrence interval. This explanation applies only to the Prince William Sound part of the 1964 earthquake rupture, as the Kodiak part of the rupture is unambiguously due to rupture of the Pacific–North America subduction interface.

If the above hypothesis is correct, then the 1964 earthquake rupture was a multifault rupture. The hypothesis implies that the rupture began on the Yakutat–North America interface, and propagated updip and bilaterally along-strike from the hypocenter beneath northern Prince William Sound. Rupture propagated eastward only as far as Kayak Island (Figure 4), before dying out. To the west, however, the rupture propagated from the Yakutat–North America interface to the Pacific–North America interface as the Yakutat block pinched out in the subsurface, or perhaps rupture on the Pacific–North America interface was dynamically triggered by rupture on the Yakutat–North America interface. The rupture then continued several hundred kilometers westward to Kodiak Island. Multifault ruptures are common for large continental earthquakes, but are not clearly documented in the case of subduction zone events. Whether this hypothesis is correct, the earthquake also clearly ruptured splay faults in Prince William Sound [*Plafker*, 1965], so the rupture of multiple distinct faults was a characteristic of the 1964 earthquake in any case.

A corollary to this hypothesis is that there must be slip on the Pacific–Yakutat interface, and thus that interface is potentially seismogenic. Such slip is also implied in the underplating model proposed by *Fuis et al.* [2008] for southern Alaska. This idea was proposed by *Perez and Jacob* [1980],

who suggested that the Pacific plate had underthrust the Yakutat terrane along much of its length, although they focused their interpretation on the southern part of the Yakutat block. Seismic reflection lines from the TACT profile clearly show the Pacific plate underthrusting the Yakutat terrane southeast of Prince William Sound [*Brocher et al*., 1994]. Although thrust earthquakes with Pacific–Yakutat orientation have not been observed except near the southern end of the Yakutat terrane [*Perez and Jacob*, 1980], the Pacific–Yakutat interface is potentially seismogenic and shallow earthquakes there could generate tsunamis.

5. ALASKA-SCALE DEFORMATION MODELS

In the mid-1990s, two papers presented Alaska-scale deformation models based on the finite element technique [*Bird*, 1996; *Lundgren et al.*, 1995]. Because these models predated the availability of GPS velocities, it is useful to evaluate them now using this new and independent data set. The comparison is, to some extent, qualitative, because these older papers did not predict velocities at GPS sites, and the predicted model velocities must be scaled from figures. Both papers were based on limited data constraints, and thus were largely driven by the assumed geometry of the problem, and by relative plate motions. Both models used the limited Holocene fault slip rate estimates and mobile VLBI data, but they treated faults in a different manner.

Lundgren et al. [1995] used a finite element mesh in the form of a spherical shell, and used the split node technique to include the effect of major crustal faults. The fault map was based on *Plafker et al.* [1994], as were fault slip rate estimates. Other constraints on the model came from prescribed relative plate motions, and from the VLBI baseline vector rates. They used only three VLBI sites, neglecting Kodiak, Sand Point, and Cape Yakataga, because of the large elastic component to the deformation of those sites. They presented four models, which differed in the fault slip rates and in the relative weights of VLBI and slip rate data. The models predict fault slip rates and velocity vectors at points, and the latter can be compared to GPS velocities as long as we are careful to account for elastic deformation; their models did not include any component of elastic strain. In coastal Alaska, the model cannot be compared to the GPS data because the elastic component from the locked subduction zone is so large.

The models presented by *Lundgren et al.* [1995] show two main features. First, in western and southwestern Alaska, the models show the region south of the Denali fault moving to the west or southwest. There is some indication of rotation in the model velocity vectors. This feature is in reasonable agreement with the later GPS observations. Second, inland from southeastern Alaska the models show a large region moving rapidly to the north–northwest, extending inboard from the Yakutat terrane collision. Predicted motions exceed 10 mm/yr relative to North America for at least a few hundred kilometers inboard from the coast, and as far as the Mackenzie Mountains in the case of one model. The GPS observations do show some motion in this direction, but at rates several times smaller. The main cause for the discrepancy between this feature of the model and the GPS observations is that *Lundgren et al.* [1995] assumed that the Yakutat terrane moved with Pacific plate velocity. This caused it to act as an indenter, causing northward-directed shortening inboard of its entire length. However, the GPS observations show that the Yakutat terrane instead moves in a significantly different direction, parallel to the Fairweather fault rather than the Pacific–North America plate motion [*Fletcher and Freymueller*, 1999, 2003]. This dramatically affects the strain pattern, and focuses contraction in the area of the St. Elias Range instead of the Coast Mountains (Figure 2).

Bird [1996] also used a finite element mesh on a spherical shell, and used a similar fault geometry and constraining data as *Lundgren et al.* [1995]. However, Bird varied the shear traction across faults by varying the coefficient of friction of the faults. Various models were run, and were scored based on their predictions of the VLBI baseline rates, fault slip vectors, and principal stress directions. However, although *Bird* [1996] used the VLBI data, he made no correction for elastic deformation from locked faults. Thus, his models were biased and included large permanent shortening of the overriding plate over the subduction zone; this means that the inferred shear traction across the subduction zone was much too large in all of his models. As a result, *Bird*'s [1996] preferred model does a very poor job of predicting the GPS data in most of the model domain.

Bird's preferred model included a dipping Transition Fault between the Yakutat terrane and the Pacific plate, and varied its shear traction from megathrust-like to being similar to crustal faults. However, the preferred model had very little slip on this fault, which made the Yakutat terrane move with nearly Pacific plate velocity. As with *Lundgren et al.* [1995], this caused the model to predict rapid northwestern motion inboard of the Yakutat terrane, along its entire inboard margin, contrary to the later GPS observations. Bird's model also predicted a rotational motion of southern Alaska south of the Denali fault. In Bird's model, this rotational motion extended as far as Kodiak Island and parts of the Alaska Peninsula. However, the rate of rotation vastly exceeds that observed, which suggests that much less stress is transferred across the megathrust, in the long term, than assumed in his model.

Bird's [1996] model also predicts arc-parallel motions on the Alaska Peninsula, Central Aleutians, and Bering Sea.

Although these motions are in places superficially similar to the GPS observations (mainly along the Alaska Peninsula), the orientation of the velocities is rotated significantly from the observed velocities, being Aleutian-arc parallel in the model but oriented more southward in the observations. Rather than a broad shear couple along the Aleutian arc, as suggested by Bird's model, we observe the motion of large rigid plates, with slip partitioning of oblique subduction limited to the forearc region over the central and eastern Aleutians [*Cross and Freymueller*, 2008]. This, again, suggests that much less stress is transmitted across the megathrust than assumed by the model.

Both of these models used the map of known Quaternary or Holocene faults from *Plafker et al*. [1994]. This map did not include a connection between the Fairweather fault in southeast Alaska and the Denali fault system in central Alaska. *Richter and Matson* [1971] proposed such a connector fault, but definitive field evidence for or against its existence has been lacking. Recently, George Plafker (personal communication, 2006) has reinterpreted geologic mapping to suggest that a connector fault is permissible, and suggested a location where it might splay off from the Fairweather fault (Figure 1b). Based on this interpretation, *Kalbas et al.* [this volume] tested models similar to that of Bird, and concluded that models including a connector fault were superior to those that did not. In our block models discussed in the next section, we assumed the existence of such a fault.

6. BLOCK MODELS

Lahr and Plafker [1980] proposed a rotating block model for the tectonics of southern Alaska, which consisted of three major blocks moving independently from the North American plate: the Wrangell, St. Elias, and Yakutat blocks. Their model harkens back to the work of *St. Amand* [1957], who explained the curvature of the Denali fault in terms of a rotating southern Alaska block. Relative motion rates for these blocks were based on Plafker's knowledge of Alaska geology, but had few quantitative constraints. However, the basic model and its predicted motions match the GPS velocities quite well. *Fletcher* [2002] took the concept of *Lahr and Plafker* [1980] and quantified the rates more precisely using the GPS data available then, and also renamed some of the blocks. We follow the naming conventions of *Fletcher* [2002], and use the names Southern Alaska block (SOAK) instead of Wrangell block, and Fairweather block instead of St. Elias block. We think these names make better geographic sense than those used originally by *Lahr and Plafker* [1980]. This section updates the model of *Fletcher* [2002] to include a Bering Plate [*Cross and Freymueller*, 2008; *Mackey et al.*, 1997]. A more detailed block model is under development for southeast Alaska and the St. Elias Range [*Elliott et al.*, 2006], but it is not included here. The model shown here uses a mix of linear velocities and angular velocities to describe the block motion, whereas the model under development uses additional data from the St. Elias Range and southeast Alaska, and describes the motion of all blocks in terms of angular velocities.

The relative block motions predict fault slip rates, which can be compared to independent estimates. Fault slip rates estimated from paleoseismology are discussed along with other constraints on the block model in section 6.1. The tectonic implications of the block model are discussed in section 6.2, and the predictions of the block model are compared to the earthquake record in section 6.3.

6.1. Block Model Constraints

In our block model, much of Alaska lies on four blocks or plates with distinct motions relative to North America, the Bering Plate, Southern Alaska block (SOAK, largely equivalent to the Wrangell block of *Lahr and Plafker* [1980]), Yakutat block, and Fairweather block. We use the term block here to represent any rigid piece of crust that moves independently of its neighboring regions. Relative motions of these blocks are shown in Figure 17 and block motions are listed in Table 3. The Bering plate includes the Bering Sea and much of western Alaska. The boundary between the Bering plate and North America is presently uncertain, although the eastern limit of the boundary is probably the zones of seismicity in the Fairbanks area [*Cross and Freymueller*, 2008; *Ruppert et al.*, this volume]. The boundary between the Bering Plate and SOAK is also uncertain, but may lie within the Tordrillo Mountains and the Western Alaska Range [*Haeussler et al*., this volume]. Both of these regions have no GPS data and limited data on the active geology. SOAK is bounded on the north and northeast by the Denali and Totschunda faults and by the Fairweather–Totschunda connector fault, and on the south by the Alaska–Aleutian megathrust and the Chugach–St. Elias fault. The Chugach–St. Elias fault is here taken to be the boundary between SOAK and the Yakutat block, which is certainly a simplification of the tectonics of the St. Elias Range [*Elliott et al.*, 2007; *Berger et al.*, in press]. The Yakutat block is bounded by the Transition Zone, Chugach–St. Elias fault, and the Fairweather fault, and the Fairweather block is bounded by the Fairweather and Denali faults. Its southeastern boundary is uncertain; nominally, we take it to be the Denali fault and its connection to the Chatham Strait fault, although GPS data show no obvious relative motion across the Chatham Strait fault. Its boundary with North America may be diffuse, or may involve faults in the rugged and ice-covered Coast Mountains not presently known to be active.

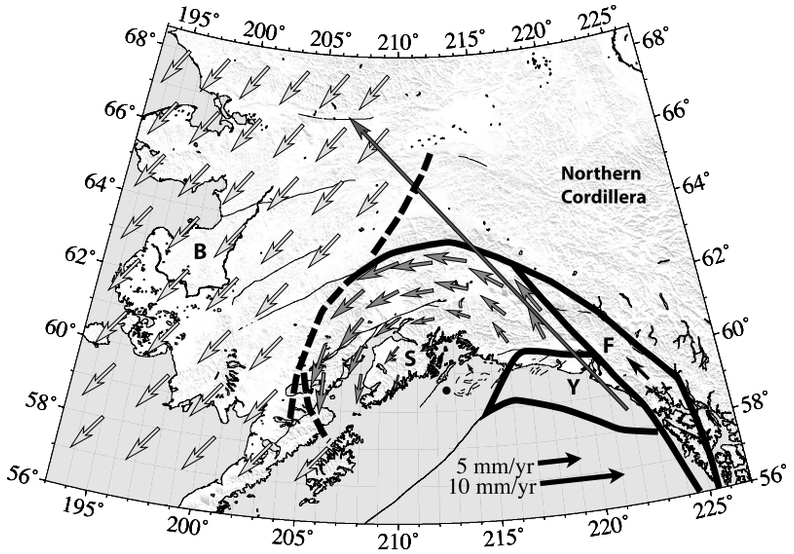

Figure 17. Block model with block velocities relative to North America. Block boundaries are shown with thick lines, and other active faults with thin lines. Block boundaries are dashed where they are indistinct or uncertain. B, Bering; S, Southern Alaska or SOAK; Y, Yakutat; F, Fairweather. The boundaries of the Bering Plate remain unknown, so the Bering–SOAK boundary is indicated using multiple dashed lines to indicate a range of plausible boundaries. Only linear velocities are estimated for the Yakutat and Fairweather blocks, whereas the vectors shown here for Bering and SOAK are based on estimated angular velocities. The solid dot just south of Prince William Sound represents the SOAK–NOAM pole of rotation.

The block motions are constrained by a variety of data. The motion of the Bering Plate is taken from *Cross and Freymueller* [2008], and the motion of SOAK from *Fletcher* [2002]. The latter is based on a pole of rotation assumed to be the pole of a small circle fit to the trace of the central Denali fault by *Stout and Chase* [1980]. The Totschunda fault lies on the same small circle about this pole as the central Denali fault. The rate of rotation of this block is based on the average Denali fault slip rate estimated from GPS data by *Fletcher* [2002], 7 mm/yr. Translation rates for the Yakutat and Fairweather blocks are based on observed GPS velocities and models fit to the Fairweather and Denali faults in southeast Alaska, 45.6 ± 2.0 and 3.8 ± 1.4 mm/yr, respectively [*Fletcher*, 2002; *Fletcher and Freymueller*, 2003]. The Denali fault slip rate assumed here is slightly slower than the recent slip rate determined by *Matmon et al.* [2006], which is based on cosmogenic dating of offset late Quaternary and Holocene features. They presented three independent measurements at two sites along the central Denali fault, which gave slip rate estimates of 7.5 ± 1.0–9.4 ± 1.2, 9.4 ± 1.3, and 9.3 ± 2.3–11.7 ± 1.8 mm/yr, respectively. In contrast, two GPS profiles across the Alaska Range show 6 ± 1 and 8 ± 1 mm/yr. Our model assigns the same slip rate to the Totschunda fault as the central Denali fault, and this rate agrees with the estimates of *Matmon et al.* [2006]. However, *Matmon et al.* [2006] and *Mériaux et al.* [2004] estimated higher slip

Table 3. Block Velocities and Angular Velocities

	Angular Velocity (°/Ma)			Linear Velocity (mm/yr)		
Block	Lat	Long	ω	V_{east}	V_{north}	Source
Bering	42.5°N	121.3°E	0.064	–	–	*Cross and Freymueller* [2008]
SOAK	59.6°N	147.4°W	–0.77	–	–	*Fletcher* [2002]
Yakutat	–	–	–	–27.4	40.7	*Elliott et al.* [2006]
Fairweather	–	–	–	–2.1	3.1	*Elliott et al.* [2006]

Block velocities are specific either by angular velocities in degrees per million years (Bering and SOAK), or linear velocities relative to North America (Yakutat and Fairweather). A positive angular velocity represents a clockwise rotation. The Bering plate angular velocity is corrected for a unit conversion error in the original publication.

rates of 12–13 mm/yr (with uncertainties of 2–4 mm/yr) at sites near the eastern part of the central Denali fault, and *Mériaux et al.* [2004] also estimated a lower slip rate of 6.6 ± 1.7 mm/yr at Bull Creek west of the 2002 Denali fault earthquake rupture zone. These authors suggested that the Denali fault slip rate decreases systematically westward, which requires partitioning of slip onto other structures, probably thrust faults oblique to the Denali fault. A significant change in the fault slip rate over the length of the central Denali fault would also require a modified pole of rotation (displaced to the west or southwest from the assumed pole), and would imply a significant contractional component across the central Denali fault. It is not easy to test this hypothesis using the GPS data, because we did not collect enough precise pre-earthquake data near the eastern part of the central Denali fault, where we have data from near the fault only at sites with two surveys 1 year apart. The two available GPS inferred slip rates are consistent with the paleoseismic rates at nearby locations. The GPS data do not support any significant contraction across the Denali fault itself, and clearly rule out rapid contraction across the fault in the west, where *Mériaux et al.* [2004] suggest that it is large.

Matmon et al. [2006] estimate a slip rate on the eastern Denali fault about 30 km east of the Denali–Totschunda junction, of 4.8–6.8 mm/yr depending on the site, which is similar to our estimate for central Denali. However, in our block model the slip rate on this fault is lower, because our data across the eastern Denali fault show only 3–4 mm/yr slip [*Fletcher and Freymueller*, 2003]. Our estimate for the eastern Denali fault comes from a very different location than that used by *Matmon et al.* [2006]. There is no obvious explanation for this difference, although the proximity of Matmon et al.'s sampling site to the Denali–Totschunda fault junction may be a cause. If so, that would suggest a decrease in the slip rate to the southeast, and require distributed deformation on one side of the fault or the other.

Despite the present limitations of the block model, both in the motions of the blocks and in their boundaries, it represents a useful first-order tectonic model for Alaska and can be used to evaluate relative motions on possible block-bounding structures. An inversion-based approach to the block model would be theoretically better than the approach used here, but is not straightforward because of complicating factors in the deformation field. The main problem is the presence of substantial postseismic deformation from the 1964 earthquake, a reliable model for which is only now being developed (Suito and Freymueller, submitted manuscript, 2008). The large time-dependent displacements from the 1998–2001 SSE also complicate a more formal modeling effort, especially because the time history of that event is not fully constrained [*Ohta et al.*, 2006]. This makes modeling the full displacements relative to North America a complex issue, subject to multiple time- and space-dependent processes. However, as shown in Figures 6 and 7, it is fairly simple to model the Denali fault itself in isolation using relative displacements to a local site. Until we are able to estimate site velocities while including calibrations for multiple time-dependent sources, a formal block modeling approach such as that used by *Wallace et al.* [2004] or *Meade and Hager* [2005] cannot be applied. Ongoing work will address this issue. An improved model for the horizontal deformation associated with GIA would allow removal of this nontectonic deformation source, and is needed to adopt a formal block modeling approach. Another limitation of the present model is that it does not account for deformation in the northern Canadian Cordillera (Figure 17), which clearly exhibits active seismicity and motion relative to North America [*Leonard et al.*, 2007, 2008; *Mazzotti et al.*, this volume], although rates of motion are low and uncertainties still relatively large. All data point toward a model in which part of the Northern Cordillera is pushed slowly to the NE in response to the collision of the Yakutat terrane [*Mazzotti and Hyndman*, 2002; *Mazzotti et al.*, this volume]. Slow deformation may also be occurring inboard of the Queen Charlotte fault along the entire length of the Canadian Cordillera [*Mazzotti et al.*, 2003, this volume]. Future work on these problems will provide a more complete picture of plate boundary deformation in all of western North America.

6.2. Block Model Implications

The St. Elias Range features the most rapid convergence within the crust in Alaska, and among the highest rates of convergence between continental blocks anywhere on Earth. The St. Elias Range occupies the boundary between the Yakutat block to the south and SOAK to the north. Rotation of SOAK explains the majority of the motion of sites north of the St. Elias Range, such as MCAR (McCarthy). However, the rapid NNW motion of the Yakutat block requires ~41–44 mm/yr convergence to occur between Yakutat and McCarthy [*Elliott et al.*, 2006, 2007]. Ongoing work in this area is aimed at identifying the main active tectonic structures that accommodate this rapid convergence and understanding how convergence is partitioned among them. However, the substantial decrease in velocity between Yakutat Bay and the Yakataga coast region (Figure 3) requires there to be active faults that reach the surface southeast of the Yakataga area. Structures in the Icy Bay area, and possibly in Yakutat Bay [*Plafker and Thatcher*, this volume] are plausible candidates.

The boundary between the Bering plate and the North American plate probably lies somewhere in central or western Alaska, and it may be diffuse [*Cross and Freymueller*,

2008]. There is a broad zone of diffuse seismicity in interior Alaska, the region north of the Alaska Range and Denali fault [*Page et al.*, 1995; *Ruppert et al.*, this volume], and the eastern limit of the Bering–North America boundary zone probably coincides with this seismicity. Most of the microseismicity locates within one of several NNE-trending bands (Figure 5). In addition, at least two $M > 7$ earthquakes occurred within this region in the first half of the 20th century. An M 7.3 event in 1937 had a left-lateral strike slip mechanism [*Fletcher and Christensen*, 1996], as have all of the other events in these zones that are large enough to compute a mechanism [*Ratchkovski and Hansen*, 2002]. The other large event in the region was a M 7.4 thrust event, located in the foothills of the Alaska Range [*Fletcher and Christensen*, 1996]. GPS velocities show low strain across the region, consistent with a low slip rate on these faults. Although the strain rate across this zone is low, the style of deformation agrees with that predicted by Bering–North America relative plate motion. This is discussed in more detail by *Ruppert et al.* [this volume].

In our block model there is no convergence between SOAK and North America across the Alaska Range, by assumption, and the slip rate on the central Denali fault is constant. Whether these two assumptions are correct has yet to be fully tested. Geology-based slip rate data support a decrease in rate to the west, whereas the GPS data do not, but the GPS data from the critical eastern end of the central Denali fault are not precise enough to determine the slip rate there. A significant along-strike decrease in slip rate is not possible without either transfer of right-lateral shear to parallel faults, or a significant net contraction across the central Alaska Range. If the paleoseismic data are taken at face value and the Denali fault slip rate decreases from ~12 to ~6 mm/yr over a distance of less than 300 km, substantial convergence across the Alaska Range would be required. This is not evident in the GPS profiles across the fault, although contraction at the rate of up to 1–2 mm/yr cannot be ruled out given the precision of the pre-earthquake data (Figures 5 and 6).

The development of the contractional belt in the northern foothills of the Alaska Range provides geologic evidence for net convergence across the Alaska Range [*Bemis*, 2004; *Lesh and Ridgway*, 2007], although the rate of convergence may be slow. These structures are most prominent from the Richardson Highway/Trans-Alaska Pipeline crossing at longitude 145°W, west to the western edge of the Kantishna Hills at longitude 152°W. The existence of the Bering plate offers an alternative, or additional, mechanism to drive convergence across this segment of the Alaska Range. If the area north of the Alaska Range were moving toward the south–southeast at some fraction of the Bering–North America plate motion rate, this would translate directly into convergence across the Denali fault in our model [*Cross and Freymueller*, 2008; *Ruppert et al.*, this volume]. Given the poles of rotation of the two blocks and the trace of the Denali fault, we would expect negligible convergence across the Denali fault west of 152°W, and increasing convergence to the east [*Ruppert et al*., this volume]. The block model also predicts a westward decrease in the slip rate on the Denali fault, as long as the north side of the Denali fault is part of the Bering plate rather than North America.

If the Denali fault continued to be the boundary between the Bering plate and SOAK in western Alaska, the poles of rotation would predict a decreasing slip rate on the fault and eventually rapid fault-normal extension. The surface trace of the Denali fault becomes less prominent west of Denali (Mt. McKinley) itself, and the slip rate probably decreases [*Haeussler*, this volume]. However, another boundary geometry is plausible and also consistent with the change in the Denali fault's surface expression, in which the boundary follows the western Alaska Range southward from Denali itself, which like the rest of the Alaska Range has been uplifted over the last ~6 million years [*Haeussler et al.*, this volume]. As suggested by the alternative geometries explored by *Fletcher* [2002], this solves one of the problems of the original model of *Lahr and Plafker* [1980]—which is where to put the western boundary of SOAK without predicting rapid extension of several mm/yr. If the Bering–SOAK boundary follows the western Alaska Range and Tordrillo Mountains, our block model predicts very slow extension across the boundary, with the Bering plate moving to the NW at a rate of 3.2 mm/yr relative to SOAK. However, this motion is not significant considering the present uncertainties in the block model. Because of the complexities in separating the subduction-related elastic strain and postseismic deformation from the block motion, we cannot yet test whether present convergence would occur across this region. Some ambiguity also remains about the location of the southern limit of SOAK. Sites on the Alaska Peninsula move consistent with Bering plate motion, and Kodiak Island may also lie on the Bering plate. Bering–SOAK relative motions differ by only ~1 mm/yr in this region, so it is presently impossible to distinguish which block these sites belong to.

6.3. The Earthquake Record, Seismic Potential, and Fault Slip Rates

Our block model can be used to make a first-order estimate of the seismic potential of the overriding plate in Alaska. To first order, the block boundaries with the highest rates of relative motion should contain the fault systems with the highest rate of large earthquakes. However, because the historical earthquake record is very short compared to the earthquake recurrence interval for most faults, the earthquake catalog

is certainly too short to completely constrain block motion rates. Nevertheless, a comparison of block motion rates estimated from the earthquake catalog to rates inferred from GPS can be enlightening. *Leonard et al.* [2008] recently estimated deformation rates from the seismicity record, and we compare our block model rates to theirs.

The block boundaries in our model were chosen based on our available knowledge of the most significant faults in the overriding plate in Alaska. Implicit in the block model is that assumption that faults within the blocks slip much more slowly than the block boundary faults, so the block boundaries should have the greatest potential to generate large earthquakes in the future. Two block boundary faults in particular have the highest seismic potential outside of the Alaska–Aleutian Megathrust: the Fairweather fault and the fault systems in the St. Elias Range. Both of these faults or fault systems have slip rates 40–45 mm/yr, which equates to 10–11 m of slip every 250 years. At such a high slip rate, $M \sim 8$ earthquakes are possible every century or so if a sufficiently long section of the fault ruptures. The Fairweather fault last ruptured in the 1958 Lituya Bay earthquake (M_w = 7.9), whereas multiple earthquakes in 1899 may have ruptured much of the St. Elias region [*Plafker and Thatcher*, this volume]. With a convergence rate in excess of 40 mm/yr, if the convergence along the entire St. Elias orogen (the Yakataga segment of Figure 1b) is taken up on a single thrust fault, then the slip deficit since 1899 is again sufficient to produce an $M \sim 8$ earthquake if the entire segment ruptured at once.

Much of the central Denali fault ruptured in a M_w = 7.9 earthquake in 2002 [*Eberhart-Phillips et al.*, 2003]. The fault segment to the west of the 2002 rupture could be long enough to rupture in a similar-sized earthquake in the future. The eastern Denali fault in Canada appears to have a lower slip rate than the central Denali fault, based on both the GPS data and the earthquake record [*Leonard et al.*, 2008]. However, even if the slip rate is only a few mm/yr, less frequent large earthquakes may be possible on this stretch of the fault, and paleoseismic investigations now underway may shed much more light on the potential of this part of the Denali fault system. The Totschunda fault is estimated to have a similar slip rate as the central Denali fault in our block model, and the inferred connector fault between the Totschunda and Fairweather faults would also have a similar rate. These faults have the potential to be significant seismic sources.

Our block model implies two additional significant seismic sources, corresponding to the Bering–North America plate boundary zone. The deformation rate across the NNE-trending left-lateral seismic zones north of the Denali fault is sufficient to account for no more than ~1/3 of the Bering–North America plate relative motion, leaving additional motion to be taken up on faults farther to the west [*Ruppert et al.*, this volume]. Diffuse seismicity across western and northwestern Alaska was part of the original basis for the Bering plate hypothesis [*Mackey et al.*, 1997], and the present GPS data in the region are not sufficient to further clarify how deformation is distributed. In addition, the block model predicts that slow but potentially significant relative motion may be occurring across the western Alaska Range, as a result of Bering–SOAK relative motion (Figure 17). There have been no historical large earthquakes in this area, and microseismicity is sparse.

Leonard et al. [2008] summed seismic moments for regions across Alaska and northwestern Canada to estimate deformation rates. Instead of a classic Kostrov-type summation of moment tensors of large earthquakes only, they use the frequency–magnitude distribution and an assumed maximum magnitude to estimate the deformation rate in each region, and make an additional assumption of the characteristic fault style. Their assumed fault styles are in all cases consistent with our block model. Their deformation rates can be compared to the GPS rates or the block model for five faults: the Fairweather fault in southeast Alaska (section 3.1, Figure 2), the eastern Denali fault in Canada (section 3.1, Figure 2), the central Denali and Totschunda faults (section 3.3, Figures 5, 6, and 7), and the seismic zones north of the Denali fault in Interior Alaska (section 3.3, Figure 5). For the eastern Denali, central Denali, and Totschunda faults, *Leonard et al.* [2008] estimated deformation rates of 2, 7–10, and 4.5 mm/yr, respectively, all in excellent agreement with the slip rate assumed in our block model. However, their estimated deformation rate for the Fairweather fault (18–27 mm/yr) is significantly slower than that observed by GPS (~45 mm/yr). This could mean that the earthquake catalog in that region is incomplete, or that their assumed maximum magnitude is wrong, or that the historical earthquake rate in that region is lower than average despite the occurrence of the 1958 Lituya Bay earthquake.

The region north of the Denali fault, around Fairbanks, is another region where the deformation rate from historical seismicity is very different from that observed by GPS. *Fletcher* [2002] estimated a total deformation rate of 2 mm/yr or less across this region, which remains a reasonable estimate given the updated velocity field shown here (Figure 5). However, *Leonard et al.* [2008] estimate a deformation rate of 8–13 mm/yr, several times higher, because of the high rates of microseismicity and the historical occurrence of $M \sim 7$ earthquakes in the region. This rate is approximately twice as large as the total Bering–North America motion [*Cross and Freymueller*, 2008]. Although it is not clear why, the seismicity rate in

this area over the last century appears to be anomalously high. Long-term earthquake clustering due to long-range fault interactions in slowly deforming regions, such as has been observed in parts of California, may explain the high seismicity rate of the last century in this region [*Dolan et al.*, 2007].

7. CONCLUSIONS

We presented a comprehensive GPS average velocity field covering the period 1992–2002 for sites near the 2002 Denali fault earthquake rupture, and 1992–2007 for sites far from the earthquake. We reviewed the major results of previously published papers that used subsets of this data, and discussed seismic cycle and tectonic models for Alaska, as well as past Alaska-scale deformation models. The spatially and temporally complex pattern of crustal deformation in Alaska results from several sources, and the complex velocity field can be explained in terms of a superposition of these sources. Most of the spatial and temporal variation in crustal deformation in Alaska can be described in terms of one or more of these four main processes: postseismic deformation after the 1964 earthquake, spatial variations in plate coupling/slip deficit, translation and rotation of large crustal blocks or plates, and a large SSE in Cook Inlet.

Postseismic deformation from the 1964 earthquake continues today, mainly caused by viscoelastic relaxation. Some continuing afterslip is still possible given the relaxation time observed in the first decade after the earthquake and the general logarithmic temporal relaxation commonly assumed for afterslip. Postseismic deformation from the 1964 earthquake causes a trenchward motion with a magnitude of 15–20 mm/yr in the Cook Inlet region, ~5 mm/yr in the Alaska Range farther inland, and 2–3 mm/yr in the Fairbanks area. This signal is almost entirely confined to the region inland from the 1964 rupture; there is little to no evidence for any along-strike propagation of the postseismic deformation.

The behavior of the shallow seismogenic zone along the Alaska–Aleutian megathrust is characterized by dramatic along-strike variability. The slip deficit along the margin and the width of the inferred seismogenic zone vary over along-strike distances that are short compared to the width. The distribution of locked and creeping regions along the megathrust is consistent with the persistent asperity hypothesis, because the locked regions estimated from the present-day GPS velocities match the asperities of the last set of great subduction zone earthquakes in Alaska. The one exception to this rule involves the 1946 Scotch Cap earthquake, which occurred in a region where we estimate a low slip deficit today. However, this earthquake was extraordinary in terms of the tsunami it generated, and may have been dominated by slip at very shallow depths near the trench, where geodetic data have poor resolution.

A large SSE occurred in upper Cook Inlet in 1998–2001, and a smaller event in the same area in 2005–2006. There is evidence for another possible SSE in lower Cook Inlet ending in 1995–1996, and weaker evidence for possible events at Kodiak Island, but no other clear-cut evidence for SSEs in Alaska. In particular, no sign of repeated SSEs has been found in segments that are dominated by creep, which suggests that creep there occurs quasi-statically.

The overriding plate in Alaska is subject to considerable internal deformation, and can be described in terms of the independent motions of four or more blocks or small plates. In the western part of Alaska and the Aleutians, the Bering plate rotates counterclockwise relative to North America about a pole of rotation located in eastern Siberia. The eastern boundary of the Bering plate is not certain, but it must lie to the west of the Fairbanks area. South-central Alaska south of the Denali fault rotates counterclockwise relative to North America about a pole located off the southern coast of Alaska. The interaction between these two blocks or plates may be responsible for the development of the western Alaska Range, and for the fold-and-thrust belt on the north side of the Alaska Range. The rotation of the Southern Alaska block is probably driven by the collision of the Yakutat block, which is colliding with southern Alaska. Inboard and northeast of the Yakutat block, the Fairweather block between the Fairweather and eastern Denali faults moves northward to northwestward relative to North America.

Acknowledgments. GPS field observations used in this paper have been the work of too many people to list here. University of Alaska Fairbanks GPS field observations have been supported by NSF grants EAR-9706318, EAR-9870144, EAR-9805326, EAR-9980496, EAR-9973189, EAR-0106824, EAR-0106829, EAR-0207957, EAR-0229934, EAR-0310410, EAR-0408799, EAR-048801, and EAR-0409950; the USGS NEHRP program; the Alaska Volcano Observatory; and the Geophysical Institute's internal funds. The NASA Dynamics of the Solid Earth program supported most of the early GPS data collection in Alaska. We thank all of the agencies and groups listed in Table 2 for sharing raw data; every person working on Alaska deformation has been willing to share raw GPS data either before or after publication, for inclusion into our unified velocity field. We thank Jeanne Sauber and Peter Haeussler in particular for numerous discussions about the tectonics and crustal deformation of Alaska. Constructive reviews by John Beavan, an anonymous reviewer, and editor Peter Haeussler helped us to significantly improve this manuscript.

REFERENCES

Abers, G. A., P. E. van Keken, E. A. Kneller, A. Ferris, and J. C. Stachnik (2006), The thermal structure of subduction zones constrained by seismic imaging: Implications for slab dehydration and wedge flow, *Earth Planet. Sci. Lett.*, *241*, 387–397.

Agnew, D. C. (1997), NLOADF: A program for computing oceantide loading, *J. Geophys. Res.*, *102*, 5109–5110.

Argus, D. F. (2007), Defining the translational velocity of the reference frame of Earth, *Geophys. J. Intl*., *169*, 830–838.

Argus, D. F., and G. A. Lyzenga (1994), Site velocities before and after the Loma Prieta and Gulf of Alaska earthquakes determined from VLBI, *Geophys. Res. Lett.*, *21*, 333–336.

Avé Lallemant, H. G., and J. S. Oldow (2000), Active displacement partitioning and arc-parallel extension of the Aleutian volcanic arc based on Global Positioning System geodesy and kinematic analysis, *Geology*, *28*, 739–742.

Beavan, J., R. Bilham, and K. Hurst (1984), Coherent tilt signals observed in the Shumagin Seismic Gap: Detection of time-dependent subduction at depth?, *J. Geophys. Res.*, *89*(B6), 4478–4492.

Beavan, J., K. Hurst, R. Bilham, and L. Shengold (1986), A densely spaced array of sea level monitors for the detection of vertical crustal deformation in the Shumagin Seismic Gap, Alaska, *J. Geophys. Res.*, *91*(B9), 9067–9080.

Bemis, S. P. (2004), Neotectonic framework of the north-central Alaska Range foothills, M.S. thesis, 153 pp., Univ. of Alaska, Fairbanks.

Bemis, S. P., and W. K. Wallace (2007), Neotectonic framework of the north-central Alaska Range foothills, in *Tectonic Growth of a Collisional Continental Margin: Crustal Evolution of Southern Alaska*, *Geol. Soc. Am. Spec. Pap.*, vol. 431, edited by K. D. Ridgway et al., pp. 549–572, GSA, Boulder, Colo., doi:10.1130/2007.2431(21).

Berger, A. L., J. A. Spotila, J. B. Chapman, T. L. Pavlis, E. Enkelmann, N. A. Ruppert, and J. T. Buscher, Architecture, kinematics, and exhumation of a convergent orogenic wedge: A thermochronological investigation of tectonic–climatic interactions within the Central St. Elias Orogen, Alaska, *Earth Planet. Sci. Lett.*, in press.

Bilek, S. L., T. Lay, and L. J. Ruff (2004), Radiated seismic energy and earthquake source duration variations from teleseismic source time functions for shallow subduction zone thrust earthquakes, *J. Geophys. Res.*, *109*, B09308, doi:10.1029/2004JB003039.

Bird, P. (1996), Computer simulations of Alaskan neotectonics, *Tectonics*, *15*, 225–236.

Boyd, T. M., and J. L. Nabelek (1988), Rupture process of the Andreanof Islands earthquake of May 7, 1986, *Bull. Seismol. Soc. Am.*, *78*(5), 1653–1673.

Boyd, T. M., J. J. Taber, A. L. Lerner-Lam, and J. Beavan (1988), Seismic rupture and arc segmentation within the Shumagin Islands Seismic Gap, Alaska, *Geophys. Res. Lett.*, *15*(3), 201–204.

Brocher, T. M., G. S. Fuis, M. A. Fisher, G. Plafker, M. J. Moses, J. J. Taber, and N. I. Christensen (1994). Mapping the megathrust beneath the northern Gulf of Alaska using wide-angle seismic data, *J. Geophys. Res.*, *99*, 11,663–11,685.

Brown, L. D., R. E. Reilinger, S. R. Holdahl, and E. I. Balazs (1977), Postseismic crustal uplift near Anchorage, Alaska, *J. Geophys. Res.*, *82*, 3369–3378.

Burris, L. (2007), Seismicity and stresses in the Kantishna seismic cluster, Central Alaska, MS thesis, 87 pp., Univ. of Alaska Fairbanks.

Calkin, P. E., G. C. Wiles, and D. J. Barclay (2001), Holocene coastal glaciation of Alaska, *Quat. Sci. Rev.*, *20*, 449–461.

Carver, G., and G. Plafker (2008), Paleoseismicity and neotectonics of the Aleutian subduction zone—An overview, this volume.

Chapman, J. B., et al., Neotectonics of the Yakutat collision: Changes in deformation driven by mass redistribution, in *Active Tectonics and Seismic Potential of Alaska, Geophys. Monogr. Ser.*, edited by J. T. Freymueller, P. J. Haeussler, R. Wesson, and G. Ekstrom, AGU, Washington, D. C., this volume.

Cohen, S. C., and J. T. Freymueller (1997), Deformation of the Kenai Peninsula, Alaska, *J. Geophys. Res.*, *102*, 20,479–20,487.

Cohen, S. C., and J. T. Freymueller (2004), Crustal deformation in Southcentral Alaska: The 1964 Prince William sound earthquake subduction zone, *Adv. Geophys.*, *47*, 1–63.

Cohen, S., S. Holdahl, D. Caprette, S. Hilla, R. Safford, and D. Schultz (1995), Uplift of the Kenai Peninsula, Alaska, since the 1964 Prince William Sound earthquake, *J. Geophys. Res.*, *100*, 2031–2038.

Crone, A. J., S. Personius, P. A. Craw, P. J. Haeussler, and L. A. Staft (2004), The Susitna Glacier thrust fault—characteristics of ruptures that initiated the 2002 Denali fault earthquake, *Bull. Seismol. Soc. Am.*, *94*(6B), S5–S22.

Cross, R. S., and J. T. Freymueller (2007), Plate coupling variation and block translation in the Andreanof segment of the Aleutian Arc determined by subduction zone modeling using GPS data, *Geophys. Res. Lett.*, *34*, L06304, doi:10.1029/2006GL028970.

Cross, R. S., and J. T. Freymueller (2008), Evidence for and implications of a Bering plate based on geodetic measurements from the Aleutians and western Alaska, *J. Geophys. Res.*, *113*, B07405, doi:10.1029/2007JB005136.

Dolan, J. F., D. D. Bowman, and C. G. Sammis (2007), Long-range and long-term fault interactions in Southern California, *Geology*, *35*, 855–858.

Eberhart-Phillips, D. et al. (2003), The 2002 Denali Fault earthquake, Alaska: A large magnitude, slip-partitioned event, *Science*, *300*, 113–119.

Eberhart-Phillips, D., D. H. Christensen, T. M. Brocher, R. Hansen, N. A. Ruppert, P. J. Haeussler, and G. A. Abers (2006), Imaging the transition from Aleutian subduction to Yakutat collision in central Alaska, with local earthquakes and active source data, *J. Geophys. Res.*, *111*, B11303, doi:10.1029/2005JB004240.

Ekström, G., and E. R. Engdahl (1989), Earthquake source parameters and stress distribution in the Adak Island region of the central Aleutian Islands, Alaska, *J. Geophys. Res.*, *94*, 15,499–15,519.

Elliott, J., J. T. Freymueller, and C. F. Larsen (2006), Using GPS to untangle the tectonics of the Saint Elias orogen, Alaska, *Eos Trans. AGU*, *87*(52), Fall Meet. Suppl., Abstract G42A-03.

Elliott, J. L., J. T. Freymueller, and B. Rabus (2007), Coseismic deformation of the 2002 Denali fault earthquake: Contributions from synthetic aperture radar range offsets, *J. Geophys. Res.*, *112*, B06421, doi:10.1029/2006JB004428.

Ferris, A., G. A. Abers, D. H. Christensen, and E. Veenstra (2003), High resolution image of the subducted Pacific (?) plate beneath central Alaska, 50–150 km depth, *Earth Planet. Sci. Lett.*, *214*, 575–588.

Fletcher, H. J. (2002), Crustal deformation in Alaska measured using the Global Positioning System, Ph.D. thesis, 135 pp., Univ. of Alaska Fairbanks.

Fletcher, H. J., and D. H. Christensen (1996), A determination of source properties of large intraplate earthquakes in Alaska, *Pure Appl. Geophys.*, *146*, 21–41.

Fletcher, H. J., and J. T. Freymueller (1999), New GPS constraints on the motion of the Yakutat block, *Geophys. Res. Lett.*, *26*, 3029–3032.

Fletcher, H. J., and J. T. Freymueller (2003), New constraints on the motion of the Fairweather fault, Alaska, from GPS observations, *Geophys. Res. Lett.*, *30*(3), 1139, doi:10.1029/2002GL016476.

Fletcher, H. J., J. Beavan, J. Freymueller, and L. Gilbert (2001), High interseismic coupling of the Alaska subduction zone SW of Kodiak Island inferred from GPS data, *Geophys. Res. Lett.*, *28*, 443–446.

Fournier, T. J., and J. T. Freymueller (2007), Transition from locked to creeping subduction in the Shumagin region, Alaska, *Geophys. Res. Lett.*, *34*, L06303, doi:10.1029/2006GL029073.

Freed, A., R. Bürgmann, E. Calais, and J. Freymueller (2006a), Stress-dependent power-law flow in the upper mantle following the 2002 Denali, Alaska, earthquake, *Earth Planet. Sci. Lett.*, *252*, 481–489.

Freed, A. M., R. Bürgmann, E. Calais, J. Freymueller, and S. Hreinsdóttir (2006b), Implications of deformation following the 2002 Denali, Alaska, earthquake for postseismic relaxation processes and lithospheric rheology, *J. Geophys. Res.*, *111*, B01401, doi:10.1029/2005JB003894.

Freymueller, J., Seasonal position variations and regional reference frame realization, GRF2006 Symposium Proceedings, in press.

Freymueller, J. T., and J. Beavan (1999), Absence of strain accumulation in the western Shumagin segment of the Alaska subduction zone, *Geophys. Res. Lett.*, *26*, 3233–3236.

Freymueller, J. T., M. H. Murray, P. Segall, and D. Castillo (1999), Kinematics of the Pacific–North America plate boundary zone, Northern California, *J. Geophys. Res*., *104*, 7419–7441.

Freymueller, J. T., S. C. Cohen, and H. J. Fletcher (2000), Spatial variations in present-day deformation, Kenai Peninsula, Alaska, and their implications, *J. Geophys. Res.*, *105*, 8079–8101.

Fuis, G. S., et al. (2008), Trans-Alaska Crustal Transect and continental evolution involving subduction underplating and synchronous foreland thrusting, *Geology*, *36*, 267–270.

Fujita, K., K. G. Mackey, R. C. McCaleb, L. V. Gunbina, V. N. Kovalev, V. S. Imaev, and V. N. Smirnov (2002), Seismicity of Chukotka, northeastern Russia, in *Tectonic Evolution of the Bering Shelf–Chukchi Sea–Arctic Margin and Adjacent Landmasses*, *Geol. Soc. Am. Spec. Pap*., vol. 360, edited by E. L. Miller, A. Grantz, and S. L. Klemperer, pp. 259–272.

Geist, E. L., J. R. Childs, and D. W. Scholl (1988), The origin of summit basins of the Aleutian ridge: Implications for block rotation of an arc massif, *Tectonics*, *7*(2), 327–341.

Gilpin, L. M. (1995), Holocene paleoseismicity and coastal tectonics of the Kodiak Islands, Alaska, Ph.D. thesis, 357 pp., Univ. of Calif., Santa Cruz.

Gilpin, L. M., G. A. Carver, S. Ward, and R. S. Anderson (1994), Tidal benchmark readings and postseismic rebound of the Kodiak Islands, SW extent of the 1964 great Alaskan earthquake rupture zone, *Seismol. Res. Lett.*, *65*(1), 68.

Gordeev, E. I., A. A. Gusev, V. E. Levin, V. F. Bakhtiarov, V. M. Pavlov, V. N. Chebrov, and M. Kasahara (2001), Preliminary analysis of deformation at the Eurasia Pacific–North America plate junction from GPS data, *Geophys. J. Int.*, *147*(1), 189–198, doi:10.1046/j.0956-540x.2001.01515.x.

Grapenthin, R., F. Sigmundsson, H. Geirsson, T. Árnadóttir, and V. Pinel (2006), Icelandic rhythmics: Annual modulation of land elevation and plate spreading by snow load, *Geophys. Res. Lett.*, *33*, L24305, doi:10.1029/2006GL028081.

Gregorius, T. (1996), *GIPSY-OASIS II: A User's Guide*, (self-published), University of Newcastle, U.K.

Griscom, A., and P. E. Sauer (1990), Interpretation of magnetic maps of the northern Gulf of Alaska with emphasis on the source of the Magnetic Slope anomaly, *U.S. Geol. Surv. Open File Rep. 90-348*, 18 pp.

Haeussler, P. J., An overview of the neotectonics of interior Alaska: Far-field deformation from the Yakutat microplate collision, this volume.

Haeussler, P. J., et al. (2004), Surface rupture and slip distribution of the Denali and Totschunda faults in the 3 November 2002 *M*7.9 earthquake, Alaska, *Bull. Seismol. Soc. Am.*, *94*(6B), S23–S52.

Haeussler, P. J., P. B. O'Sullivan, A. L. Berger, and J. A. Spotila, Neogene exhumation of the Tordrillo Mountains, Alaska, and correlations with Denali (Mt. McKinley), this volume.

Heki, K. (2003), Snow load and seasonal variation of earthquake occurrence in Japan, *Earth Planet. Sci. Lett*., *207*, 159–164.

Holdahl, S. R., and J. Sauber (1994), Coseismic slip in the 1964 Prince William Sound Earthquake: A new geodetic inversion, *Pure Appl. Geophys*., *142*, 55–82.

Houston, H., and E. R. Engdahl (1989), A comparison of the spatio-temporal distribution of moment release for the 1986 Andreanof Islands earthquake with relocated seismicity, *Geophys. Res. Lett.*, *16*(12), 1421–1424.

Hreinsdóttir, S., J. T. Freymueller, R. Bürgmann, and J. Mitchell (2006), Coseismic deformation of the 2002 Denali Fault earthquake: Insights from GPS measurements, *J. Geophys. Res.*, *111*, B03308, doi:10.1029/2005JB003676.

Hurst, K., and J. Beavan (1987), Improved sea level monitors for measuring vertical crustal deformation in the Shumagin Seismic Gap, Alaska, *Geophys. Res. Lett.*, *14*(12), 1234–1237.

Ichinose, G., P. Somerville, H. K. Thio, R. Graves, and D. O'Connell (2007), Rupture process of the 1964 Prince William Sound, Alaska, earthquake from the combined inversion of seismic, tsunami, and geodetic data, *J. Geophys. Res.*, *112*, B07306, doi:10.1029/2006JB004728.

Johnson, J. M., Y. Tanioka, L. Ruff, K. Satake, H. Kanamori, and L. Sykes (1994), The 1957 Great Aleutian Earthquake, *Pure Appl. Geophys.*, *142*(1), 3–28.

Johnson, J. M., K. Satake, S. R. Holdahl, and J. Sauber (1996), The 1964 Prince William Sound earthquake: Joint inversion of tsunami and geodetic data, *J. Geophys. Res.*, *101*, 523–532.

Kalbas, J. L., A. M. Freed, and K. D. Ridgway, Contemporary fault mechanics in southern Alaska: Neotectonics of Alaska, in this volume.

Kataoka, T., and K. Heki (2007), Biannually repeating slow slip events in an uncoupled segment of the Ryukyu Arc, SW Japan, *Eos Trans. AGU*, *88*(52), Fall Meet. Suppl., Abstract G21C-0674.

Lahr, J. C., and G. Plafker (1980), Holocene Pacific–North American Plate interaction in southern Alaska; Implications for the Yakataga seismic gap, *Geology*, *8*, 483–486.

Larsen, C. F., R. J. Motyka, J. T. Freymueller, K. A. Echelmeyer, and E. R. Ivins (2004), Rapid uplift of southern Alaska caused by recent ice loss, *Geophys. J. Int.*, *158*, 1118–1133.

Larsen, C. F., R. J. Motyka, J. T. Freymueller, K. A. Echelmeyer, and E. R. Ivins (2005), Rapid viscoelastic uplift in southeast Alaska caused by post-Little Ice Age glacial retreat, *Earth Planet. Sci. Lett.*, *237*, 548–560.

Larson, K. M., and M. Lisowski (1994), Strain accumulation in the Shumagin Islands: Results of initial GPS measurements, *Geophys. Res. Lett.*, *21*(6), 489–492.

Larson, K. M., J. T. Freymueller, and S. Philipsen (1997), Global plate velocities from the Global Positioning System, *J. Geophys. Res*., *102*, 9961–9982.

Leonard, L. J., R. D. Hyndman, S. Mazzotti, L. Nykolaishen, M. Schmidt, and S. Hippchen (2007), Current deformation in the northern Canadian Cordillera inferred from GPS measurements, *J. Geophys. Res.*, *112*, B11401, doi:10.1029/2007JB005061.

Leonard, L. J., S. Mazzotti, and R. D. Hyndman (2008), Deformation rates estimated from earthquakes in the northern Cordillera of Canada and eastern Alaska, *J. Geophys. Res.*, *113*, B08406, doi:10.1029/2007JB005456.

Lesh, M. E., and K. D. Ridgway (2007), Geomorphic evidence of active transpressional deformation in the Tanana foreland basin, south-central Alaska, in *Tectonic Growth of a Collisional Continental Margin: Crustal Evolution of Southern Alaska*, *Geol. Soc. Am. Spec. Pap.*, vol. 431, doi:10.1130/2007.2431(22).

Lisowski, M., J. C. Savage, and R. O. Burford (1987), Strain accumulation across the Fairweather and Totschunda faults, Alaska, *J. Geophys. Res.*, *92*(B11), 11,552–11,560.

Lisowski, M., J. C. Savage, W. H. Prescott, and W. K. Gross (1988), Absence of strain accumulation in the Shumagin Seismic Gap, Alaska, 1980–1987, *J. Geophys. Res.*, *93*(B7), 7909–7922.

López, A. M., and E. A. Okal (2006), A seismological reassessment of the source of the 1946 Aleutian "tsunami" earthquake, *Geophys. J. Int.*, *165*, 835–849.

Lu, Z., and M. Wyss (1996), Segmentation of the Aleutian plate boundary derived from stress direction estimates based on fault plane solutions, *J. Geophys. Res.*, *101*(B1), 803–816.

Lu, Z., D. Mann, J. T. Freymueller, and D. J. Meyer (2000a), Synthetic aperture radar interferometry of Okmok volcano, Alaska: Radar observations, *J. Geophys. Res.*, *105*, 10,791–10,806.

Lu, Z., C. Wicks, D. Dzurisin, W. Thatcher, J. T. Freymueller, S. R. McNutt, and D. Mann (2000b), Aseismic inflation of Westdahl volcano, Alaska, revealed by satellite radar interferometry, *Geophys. Res. Lett.*, *27*, 1567–1570.

Lu, Z., C. Wicks Jr., J. A. Power, and D. Dzurisin (2000c), Ground deformation associated with the March 1996 earthquake swarm at Akutan volcano, Alaska, revealed by satellite radar interferometry, *J. Geophys. Res.*, *105*(B9), 21,483–21,495.

Lu, Z., T. Masterlark, and D. Dzurisin (2005), Interferometric synthetic aperture radar study of Okmok volcano, Alaska, 1992–2003: Magma supply dynamics and postemplacement lava flow deformation, *J. Geophys. Res.*, *110*, B02403, doi:10.1029/2004JB003148.

Lundgren, P., F. Saucier, R. Palmer, and M. Langon (1995), Alaska crustal deformation: Finite element modeling constrained by geologic and very long baseline interferometry data, *J. Geophys. Res*., *100*, 22,033–22,046.

Ma, C., J. M. Sauber, L. J. Bell, T. A. Clark, D. Gordon, W. E. Himwich, and J. W. Ryan (1990), Measurement of horizontal motions in Alaska using very long baseline interferometry, *J. Geophys. Res.*, *95*(B13), 21,991–22,011.

Mackey, K., K. Fujita, L. Gunbina, V. Kovalev, V. Imaev, B. Koz'min, and L. Imaeva (1997), Seismicity of the Bering Strait region: Evidence for a Bering block, *Geology*, *25*(11), 979–982.

Mann, D., and J. Freymueller (2003), Volcanic and tectonic deformation on Unimak Island in the Aleutian Arc, Alaska, *J. Geophys. Res.*, *108*(B2), 2108, doi:10.1029/2002JB001925.

Matmon, A., D. P. Schwartz, P. J. Haeussler, R. Finkel, J. J. Lienkaemper, H. D. Stenner, and T. E. Dawson (2006), Denali fault slip rates and Holocene–late Pleistocene kinematics of central Alaska, *Geology*, *34*, 645–648, doi:10.1130/G22361.1.

Mazzotti, S., and R. Hyndman (2002), Yakutat collision and strain transfer across the northern Canadian Cordillera, *Geology*, *30*, 495–498.

Mazzotti, S., R. D. Hyndman, P. Flück, A. J. Smith, and M. Schmidt (2003), Distribution of the Pacific/North America motion in the Queen Charlotte Islands-S. Alaska plate boundary zone, *Geophys. Res. Lett*., *30*(14), 1762, doi:10.129/2003GL017586.

Mazzotti, S., L. J. Leonard, R. D. Hyndman, and J. F. Cassidy, Tectonics, dynamics, and seismic hazard in the Canada–Alaska Cordillera, this volume.

McCaffrey, R. (1992) Oblique plate convergence, slip vectors, and forearc deformation, *J. Geophys. Res.*, *97*, 8905–8915.

McCaffrey, R. (2002), Crustal block rotations and plate coupling, in *Plate Boundary Zones*, *Geodyn. Ser.*, vol. 30, edited by S. Stein and J. T. Freymueller, pp. 101–122, AGU, Washington, D. C.

McCaffrey, R., M. D. Long, C. Goldfinger, P. C. Zwick, J. L. Nabelek, C. K. Johnson and C. Smith (2000), Rotation and plate locking at the southern Cascadia subduction zone, *Geophys. Res. Lett.*, *27*, 3117–3120.

McCaffrey, R., L. M. Wallace, and J. Beavan (2008), Slow slip and frictional transition at low temperature at the Hikurangi subduction zone, *Nat. Geosci.*, *1*, 316–320, doi:10.1038/ngeo178.

Meade, B. J., and B. H. Hager (2005), Block models of crustal motion in southern California constrained by GPS measurements, *J. Geophys. Res.*, *110*, B03403, doi:10.1029/2004JB003209.

Mériaux, A., K. Sieh, C. M. Rubin, F. J. Ryerson, R. C. Finkel, A. Meltzner, and M. Taylor (2004), Kinematics of the southern Alaska constrained by westward-decreasing post-glacial slip-rates on the Denali fault, Alaska, *Eos Trans. AGU*, *85*(47), Fall Meet. Suppl., Abstract G13C-07.

Miyagi, Y., J. T. Freymueller, F, Kimata, T. Sato, and D. Mann (2004), Surface deformation caused by shallow magmatic activity at Okmok Volcano, Alaska, detected by GPS campaigns 2000–2002, *Earth Planets Space*, *56*, e29–e32.

Motyka, R. J. (2003), Little Ice Age subsidence and Post Little Ice Age uplift at Juneau, Alaska inferred from dendrochronology and geomorphology, *Quat. Res.*, *59*, 300–309.

Niell, A. E. (1996), Global mapping functions for the atmospheric delay at radio wavelengths, *J. Geophys. Res*., *101*, 3227–3246.

Ohta, Y., J. T. Freymueller, S. Hreinsdóttir, and H. Suito (2006), A large slow slip event and the depth of the seismogenic zone in the south central Alaska subduction zone, *Earth Planet. Sci. Lett.*, *247*, 108–116.

Ohta, Y., J. T. Freymueller, and S. Miura (2007), The time constant variations of slow slip events in the south Alaska subduction zone, *Eos Trans. AGU*, *88*(52), Fall Meet. Suppl., Abstract T21A-0364.

Page, R. A., G. Plafker, and H. Pulpan (1995), Block rotation in east-central Alaska: A framework for evaluating earthquake potential?, *Geology*, *23*, 629–632.

Pavlis, T. L., C. Picornell, L. Serpa, R. L. Bruhn, and G. Plafker (2004), Tectonic processes during oblique collision: Insights from the St. Elias orogen, northern North American Cordillera, *Tectonics*, *23*, TC3001, doi:10.1029/2003TC001557.

Penna, N. T., M. A. King, and M. P. Stewart (2007), GPS height time series: Short-period origins of spurious long-period signals, *J. Geophys. Res.*, *112*, B02402, doi:10.1029/2005JB004047.

Perez, O. J., and K. H. Jacob (1980), Tectonic model and seismic potential of the eastern Gulf of Alaska and Yakataga seismic gap, *J. Geophys. Res.*, *85*(B12), 7132–7150.

Péwé, T. L. (1975), Quaternary geology of Alaska, *U.S. Geol. Surv. Prof. Pap. 835*, 145 pp., 3 sheets, scale 1:500,000.

Plafker, G. (1965), Tectonic deformation associated with the 1964 Alaska earthquake, *Science*, *148*, 1675–1687.

Plafker, G., and H. C. Berg (1994), Overview of the geology and tectonic evolution of Alaska, in *The Geology of Alaska*, *Geology of North America*, vol. G-1, edited by G. Plafker and H. C. Berg, pp. 989–1021, Geol. Soc. of Am., Boulder, Colo.

Plafker, G., and W. Thatcher, Geological and geophysical evaluation of the mechanisms of the great 1899 Yakutat Bay Earthquakes, this volume.

Plafker, G., T. Hudson, and D. H. Richter (1977), Preliminary observations on late Cenozoic displacements along the Totschunda and Denali fault systems, *Geol. Surv. Circ. U.S.*, *751B*, B67–B69.

Plafker, G., T. Hudson, T. Bruns, and M. Rubin (1978), Late quaternary offsets along the Fairweather fault and crustal plate interactions in southern Alaska, *Can. J. Earth Sci.*, *15*(5), 805–816.

Plafker, G., K. R. Lajoie, and M. Rubin (1992), Determining the recurrence intervals of great subduction zone earthquakes in southern Alaska by radiocarbon dating, in *Radiocarbon After Four Decades*, edited by R. E. Taylor, A. Long, and R. Kra, p. 27, Univ. of Arizona Press, Tucson.

Plafker, G., L. M. Gilpin, and J. C. Lahr (1994), Neotectonic map of Alaska, in *The Geology of Alaska, The Geology of North America*, vol. G1, edited by G. Plafker and H. C. Berg, Geol. Soc. of Am., Boulder, Colo., Plate 12, 1 sheet with text, scale 1:2,500,000.

Ratchkovski, N., and R. Hansen (2002), New constraints on tectonics of interior Alaska: Earthquake locations, source mechanisms, and stress regime, *Bull. Seismol. Soc. Am.*, *92*(3), 998–1014.

Richter, D. H., and N. A. Matson Jr. (1971), Quaternary faulting in the eastern Alaska Range, Alaska, *Geol. Soc. Am. Bull.*, *82*, 1529–1540.

Rogers, G., and H. Dragert (2003), Episodic tremor and slip on the Cascadia subduction zone: The chatter of silent slip, *Science*, *300*, 1942–1943.

Ruppert, N. A., K. D. Ridgway, J. T. Freymueller, R. S. Cross, and R. A. Hansen, Active tectonics of interior Alaska: A synthesis of seismic, GPS and geomorphic studies, this volume.

Sauber, J., S. McClusky, and R. King (1997), Relation of ongoing deformation rates to the subduction zone process in southern Alaska, *Geophys. Res. Lett.*, *24*, 2853–2856.

Sauber, J., G. Carver, S. Cohen, and R. King (2006), Crustal deformation and the seismic cycle across the Kodiak Islands, Alaska, *J. Geophys. Res.*, *111*, B02403, doi:10.1029/2005JB003626.

Sauber, J. M., T. A. Clark, L. J. Bell, M. Lisowski, C. Ma, and D. S. Caprette (1993), Geodetic measurement of static displacement associated with the 1987–1988 Gulf of Alaska earthquakes, in *Contributions of Space Geodesy to Geodynamics: Crustal Dynamics*, *Geodyn. Ser*., vol. 23, edited by D. E. Smith and D. L. Turcotte, pp. 233–248, AGU, Washington, D. C.

Savage, J. C. (1983), A dislocation model of strain accumulation and release at a subduction zone, *J. Geophys. Res.*, *88*, 4984–4996.

Savage, J. C., and M. Lisowski (1986), Strain accumulation in the Shumagin Seismic Gap, Alaska, *J. Geophys. Res.*, *91*(B7), 7447–7454.

Savage, J. C., and M. Lisowski (1988), Deformation in the Yakataga Seismic Gap, southern Alaska, 1980–1986, *J. Geophys. Res.*, *93*(B5), 4731–4744.

Savage, J. C., and M. Lisowski (1991), Strain accumulation along the Denali Fault at the Nenana River and Delta River crossings, Alaska, *J. Geophys. Res.*, *96*(B9), 14,481–14,492.

Savage, J. C., and G. Plafker (1991), Tide gage measurements of uplift along the south coast of Alaska, *J. Geophys. Res.*, *96*, 4325–4335.

Savage, J. C., M. Lisowski, and W. H. Prescott (1981), Strain accumulation across the Denali Fault in the Delta River Canyon, Alaska, *J. Geophys. Res.*, *86*(B2), 1005–1014.

Savage, J. C., J. L. Svarc, W. H. Prescott, and W. K. Gross, (1998) Deformation across the rupture zone of the 1964 Alaska earthquake, 1993–1997, *J. Geophys. Res.*, *103*, 21,275–21,283.

Savage, J. C., J. L. Svarc, and W. H. Prescott (1999), Deformation across the Alaska-Aleutian subduction zone near Kodiak, *Geophys. Res. Lett.*, *26*, 2117–2120.

Schwartz, S. Y., and J. M. Rokosky (2007), Slow slip events and seismic tremor at circum-Pacific subduction zones, *Rev. Geophys.*, *45*, RG3004, doi:10.1029/2006RG000208.

Sella, G. F., T. H. Dixon, and A. Mao (2002), REVEL: A model for recent plate velocities from space geodesy, *J. Geophys. Res.*, *107*(B4), 2081, doi:10.1029/2000JB000033.

Sella, G. F., S. Stein, T. H. Dixon, M. Craymer, T. S. James, S. Mazzotti, and R. K. Dokka (2007), Observation of glacial isostatic adjustment in "stable" North America with GPS, *Geophys. Res. Lett.*, *34*, L02306, doi:10.1029/2006GL027081.

Song, T.-R. A., and M. Simons (2003), Large, trench-parallel gravity variations predict seismogenic behavior in subduction zones, *Science*, *301*, 630–633.

St. Amand, P. (1957), Geological and geophysical synthesis of the tectonics of portions of British Columbia, the Yukon Territory, and Alaska, *Geol. Soc. Am. Bull.*, *68*, 1343–1370.

Stout, J. H., and C. G. Chase (1980), Plate kinematics of the Denali fault system, *Can. J. Earth Sci.*, *17*, 1527–1537.

Suito, H., J. T. Freymueller, and S. C. Cohen (2003), 3-D Viscoelastic FEM modeling of postseismic deformation caused by the 1964 Alaska Earthquake, southern Alaska, 2003 IUGG General Assembly, JSG01/08P/D-014.

Suwa, Y., S. Miura, A. Hasegawa, T. Sato, and K. Tachibana (2006), Interplate coupling beneath NE Japan inferred from three-dimensional displacement field, *J. Geophys. Res.*, *111*, B04402, doi:10.1029/2004JB003203.

Thatcher, W. (1990), Order and diversity in the modes of circum-Pacific earthquake recurrence, *J. Geophys. Res*., *95*, 2609–2623.

Veenstra, E., D. Christensen, G. A. Abers, and A. Ferris (2006), Crustal thickness variation in south central Alaska: Results from the broadband experiment across the Alaska range, *Geology*, *34*, 781–784.

von Huene, R., D. Klaeschen, and J. Fruehn (1999). Relation between the subducting plate and seismicity associated with the great 1964 Alaska earthquake, *Pure Appl. Geophys.*, *154*, 575–591.

Wallace, L. M., J. Beavan, R. McCaffrey, and D. Darby (2004), Subduction zone coupling and tectonic block rotations in the North Island, New Zealand, *J. Geophys. Res.*, *109*, B12406, doi:10.1029/2004JB003241.

Wallace, L., R. McCaffrey, J. Beavan, and S. Ellis (2005), Rapid microplate rotations and backarc rifting at the transition between collision and subduction, *Geology*, *33*, 857–860.

Wells, R. E., R. J. Blakely, Y. Sugiyama, D. W. Scholl, and P. A. Dinterman (2003), Basin-centered asperities in great subduction zone earthquakes: A link between slip, subsidence, and subduction erosion?, *J. Geophys. Res.*, *108*(B10), 2507, doi:10.1029/2002JB002072.

Wiles, G. C., D. J. Barclay, and P. E. Calkin (1999), Tree-ring-dated Little Ice Age histories of maritime glaciers from western Prince William Sound, Alaska, *The Holocene*, *9*, 163–173.

Zheng, G., R. Dmowska, and J. R. Rice (1996), Modeling earthquake cycles in the Shumagin subduction segment, Alaska, with seismic and geodetic constraints*, J. Geophys. Res.*, *101*, 8383–8392.

Zumberge, J. F., M. B. Heflin, D. C. Jefferson, M. M. Watkins, and F. H. Webb (1997), Precise point positioning for the efficient and robust analysis of GPS data from large networks, *J. Geophys. Res*., *102*, 5005–5018.

Zweck, C., J. T. Freymueller, and S. C. Cohen (2002), Elastic dislocation modeling of the postseismic response to the 1964 Alaska Earthquake, *J. Geophys. Res.*, *107*(B4), 2064, doi:10.1029/2001JB000409.

S. C. Cohen, Planetary Dynamics Laboratory, NASA Goddard Space Flight Center, Greenbelt, MD 20771, USA.

R. Cross, Tetra Tech Inc., 1917 First Avenue, Seattle, WA, USA.

J. Elliott, J. T. Freymueller, C. F. Larsen, and H. Woodard, Geophysical Institute, University of Alaska Fairbanks, 903 Koyukuk Drive, Fairbanks, AK 99775, USA. (jeff@giseis.laska.edu)

S. Hreinsdóttir, Department of Geosciences, University of Arizona, Gould-Simpson Building #77, 1040 East 4th Street, Tucson, AZ 85721, USA.

C. Zweck, Department of Hydrology and Water Resources, University of Arizona, Tucson, AZ 86721, USA.